

RESEARCH ARTICLE

An Effective Strategy for Collision Avoidance of Multiple UAVs With Unknown Acceleration

JIANWU TAO¹, SHIRU GUO¹, AND YUFENG SHANG²¹Changchun College of Electronic Technology, Changchun, Jilin 130000, China²Department of Mathematics, Aviation University of Air Force, Changchun, Jilin 130022, China

Corresponding author: Jianwu Tao (732410427@qq.com)

This work was supported in part by the Natural Science Foundation of Jilin Province, China, under Grant 20210101171JC; and in part by the National Natural Science Foundation of China under Grant 61571462.

ABSTRACT In this article, an effective strategy using mixed 3-D geometric and the miss distance approach is proposed for the collision avoidance between multiple UAVs with unknown acceleration. At each time sampling, conflict detection of multiple UAVs is first performed. If the conflict exists, the expected heading angle or/and expected elevation angle of UAV are computed. Then, UAV begins to perform the avoidance maneuvers. The heading angle or/and elevation angle of UAV are uniformly adjusted to the expected value. The condition required for successful collision avoidance is derived for the proposed strategy. To enhance safety during execution of avoidance maneuver, a simple and feasible modify measure is presented. In the case of multiple UAVs, a logic to allocate the avoidance prioritization of each UAV is proposed. The trajectory recovery algorithm is presented to ensure UAV to return to the planning flight paths. For the proposed strategy, it is not assumed that all UAVs have constant ground speeds and direction of the velocity. Thus, it is very suitable in reality application. Numerical simulation results show the efficiency and superiority of the proposed strategy.


INDEX TERMS Collision avoidance, trajectory recovery, prioritization logic, multiple UAVs, 3-D space.

I. INTRODUCTION

The use of Unmanned Aerial Vehicles (UAVs) increased significantly in the last decade. A rapid increase in the number of aircraft causes dense air traffic and may increase the risk of collision. Therefore, the collision avoidance has become increasingly important for the safe operation of UAVs. Particularly, the collision avoidance between the UAV itself and other UAVs is a challenging issue in the case of multiple UAVs.

The collision avoidance process consists of state sensing, conflict detection and conflict resolution [1], [2]. The state sensing enables the acquisition of state information on the surrounding environment, such as aircraft position, velocity and the number of intruders. Based on the sensed data, the conflict detection approach extracts useful information and is used to determine whether a potential conflict will

occur or not. In [3], the collision cone was proposed as an effective approach of conflict detection. This approach determines a collision condition by using the relation of position, velocity and heading between the obstacle and the UAV. Nowadays, the detection approaches based on collision cone are widely applied to the three-dimensional (3-D) collision avoidance for a pair of UAVs [4], [5] and multiple UAVs [6]. In [7], a straight line conflict detection and alerting algorithm was proposed for multiple unmanned aerial vehicles. This approach views the immediate trajectory as a straight line and does not require the prior knowledge of the UAVs trajectory plans. Based on the miss distance in point of closest approach, another effective approach of conflict detection was proposed in [8] and [9]. In this approach, the miss distance in point of closest approach is first computed for a pair of UAVs. Then, the miss distance is compared with a threshold distance to decide whether a conflict exists or not. In [10], the suspicious collision point is identified by using a closed-form solution of the expected miss distance between

The associate editor coordinating the review of this manuscript and approving it for publication was Guillermo Valencia-Palomo .

two UAVs. The advantage of above-mentioned approaches is its computational efficiency. In [11], the aiming point approach was proposed to determine whenever the UAV is on a collision course with the obstacle. In this approach, all possible points of avoidance trajectory are collected to form aiming point candidates, and an avoidance maneuver is performed by following the aiming point selected among the candidates. Based on the aiming point approach, a collision avoidance strategy that explicitly takes account of obstacle movement predicted for a predefined period was presented in [12]. However, the aiming point approach requires a heavy computational load to calculate all possible aiming points. This prevents its application in real-time systems.

The approaches for conflict resolution can be briefly divided into four categories: geometric-based, potential field, numerical optimization and sense-and-avoid (SAA) [1]. Geometric-based approaches rely on the analysis of geometric attributes to make sure that the defined minimum distance between two UAVs is not breached. In 2-D conflict scenario, a geometric-based resolution was used for the collision avoidance of a pair fixed-wing UAVs [9]. In [13] and [14], the geometric-based resolution was applied to the 3-D environment. In [13], the algorithms of changing independently the airspeed, heading and elevation angles were presented and all combinations of these degrees of freedom were investigated. In [14], a fast 3-D geometric avoidance algorithm was proposed for multiple fixed-wing UAVs. The artificial potential field (APF) approaches are formulated by assigning a potential function to the free space, while the aircraft is regarded as a particle reacting to attractive and repulsive forces. In the formation control of multiple UAVs, the APF approach is used to avoid the obstacles in a 3-D space [15], [16]. To achieve multi-UAV collaborative trajectory planning and collision avoidance, an optimized APF approach was proposed in [17]. This approach solves the unreachable targets problem of the traditional APF approach, so that each UAV can avoid collision with obstacles by changing its trajectory. In [18], an improved APF method for a multi-UAV system was presented to solve the path planning and formation control in 3D constrained space. In [19], a collision avoidance and formation control algorithm for a large-scale fixed-wing UAV swarm system was proposed based on the improved APF function and new swarm structure. By using the distributed control architecture of the swarm system, this algorithm can be applied in a large-scale fixed-wing UAV swarm system. The numerical optimization approaches employ a kinematic model of the aircraft together with a set of constraints and cost function. An optimal trajectory to resolve conflict is generated based on the lowest cost and the most desired constraints. In [20], a predictable collision avoidance algorithm was proposed for a pair of UAVs. In [21], conflicts among multiple UAVs are resolved by applying the local centralized optimization method with consideration given to the dynamic constraints of UAVs. The SAA approach prevents a collision by changing the travel direction of the

aircraft away from the obstacle. By simplifying the process of collision avoidance to individual detection and avoidance of obstacles, the SAA approach has low computational requirements and short response times. In [22], a conflict alerting logic integrated with the prioritization of avoidance was proposed for SAA systems. By comparing the time estimate to collision with a given threshold, it is determined whether the avoidance maneuver begins. In [23], collision avoidance strategy was proposed for UAVs in formation flight. In this strategy, a simple algorithm with low computational requirements is obtained by expanding the mixed geometric and collision cone approach to formations of UAVs. In addition, the artificial intelligence algorithms are widely used in the collision avoidance of UAV formation and UAV swarms [24], [25], [26], [27], [28]. Based on the optimized flocking model with collision avoidance, a conflict resolution for UAV swarms was developed in [24]. Based on consensus algorithm and strategy coordination, a distributed conflict detection and resolution method for UAV swarms was proposed in [25]. For solving optimization problems, an overview of the various swarm intelligence algorithms and their advanced development was provided in [26]. Based on swarm intelligence algorithm, a multi-UAV cooperative task reallocation algorithm with target precedence constraints was proposed in [27]. Based on the neural networks and the deterministic learning, the cooperative formation control method with collision avoidance was proposed in [28]. The collision avoidance methods for unknown moving obstacles were also developed in recent years. In [29], the geometric shape of unknown moving obstacles is determined by using distance and angle measurements. By combining the geometric shape of obstacles with the distance and velocity information of obstacles, critical obstacles in the environment are identified. Further, the collision avoidance between UAV and critical obstacles is achieved by using course change and velocity change. In [12], the trajectory of unknown moving obstacles is predicted by using discrete-time Kalman filtering. Based on the prediction of obstacle trajectory, a reactive collision avoidance algorithm was proposed to avoid multiple moving obstacles. To predict the positions of unknown moving obstacles flying around UAV, a trajectory evaluation algorithm based on a Markov chain with a grid map was proposed in [30]. Further, a dynamic path planning algorithm was proposed based on obstacles' position prediction and modified APF. In [31], a data-driven risk-aware approach was proposed for moving obstacle avoidance. By given measurements of the priori unknown moving obstacles, the dynamics of moving obstacles are discovered. A set of obstacle trajectories are forecasted based on bootstrap technique. By using a risk-aware model predictive control scheme, the probability guarantee on obstacle avoidance is provided.

Unfortunately, most of collision avoidance approaches above-mentioned suppose that the velocity of moving obstacles is constant when the conflict happens. In reality, there may be moving obstacles with time-varying velocity

in an unknown environment. Thus, the real-time collision avoidance is a key issue for the safe flight of UAV in a dynamic airspace. In [32], a linear time-varying collision avoidance model is established, where the acceleration of UAV implemented avoidance maneuver is used as the control input of system and the acceleration of moving obstacle is regarded as the disturbance of system. Then, a fast finite-time convergent (FFTC) guidance law with nonlinear disturbance observer was proposed. Based on dynamic APF (DAFP) algorithm, Du et al. [33] proposed a real-time reactive path planning method for collision avoidance of the UAVs. In a variety of encounter scenes, this method can generate a safe, stable, robust and flyable collision-free path for UAV flying in dynamic airspace. However, two approaches above-mentioned need to set 6 unknown coefficients in algorithm. Therefore, how to select these coefficients in advance is a tough job. Since these coefficients have different optimal values for different encounter scenes, these coefficients selected in advance is hard to satisfy all of scenes. In some cases, the improper coefficients result in the degradation of avoidance validity, or even fail. In addition, the approach proposed in [33] achieves the collision avoidance of UAV by changing the heading angle and speed of UAV. For a fixed-wing UAV, the change of speed has limited and it consumes more energy than the change of angle.

To solve above problem, an effective strategy using mixed 3-D geometric and the miss distance approaches is proposed for the real-time collision avoidance between multiple UAVs with unknown acceleration. The main contributions of this paper are following. First, a collision avoidance strategy is proposed for multiple UAVs with unknown acceleration. Different from the approaches in [32] and [33], the coefficients selected in advance and the nonlinear disturbance observer are not needed in this strategy. In addition, this approach adopts only the change of angles to achieve the collision avoidance. These imply that the proposed approach is simple in implement. And it is also energy-saving due to no change of velocity's magnitude. Second, the condition required for successful collision avoidance is derived in theory. It is very important for ensuring the efficiency of the proposed strategy. Third, the priority logic of the collision avoidance for multiple UAVs are presented based on the fusion of the miss distance and the time to closest approach. Compared with alone time-based prioritization logic [34], this logic is easier to determine the risk level of collision for each UAV. Fourth, different trajectory recovery approaches corresponding with different cases are designed to ensure UAV to return to planning flight paths rapidly. The proposed strategy does not assume that UAV and moving obstacles have a constant ground speed and direction of the velocity. Thus, it is very suitable in reality application.

II. CONFLICT DETECTION

It is assumed that two UAVs are in an encounter with each other. The geometric configuration of two UAVs in a 3-D space is illustrated in Fig. 1. Here, a UAV denoted

by "UAV(a)" is a point object. Another UAV denoted by "UAV(b)" is a sphere object with radius r_{safe} . The radius r_{safe} is the safety boundary that guarantees the safety of two UAVs. In fact, r_{safe} can also be the sum of both UAVs' radii, and is a constant determined by the designer. It is assumed that the position and velocity of UAVs, which can be obtained by collaborative or non-collaborative SAA technology [1], are known, but the acceleration of UAVs is unknown. Thus, the relative velocity vector of two UAVs can be written as

$$\mathbf{V}_{ab}(t) = \mathbf{V}_b(t) - \mathbf{V}_a(t) \quad (1)$$

where $\mathbf{V}_a(t)$ and $\mathbf{V}_b(t)$ are the velocity vector of UAV(a) and UAV (b) at time t , respectively. The line-of-sight (LOS) vector between two UAVs can be written as

$$\mathbf{R}_{los}(t) = \mathbf{P}_b(t) - \mathbf{P}_a(t) \quad (2)$$

where $\mathbf{P}_a(t)$ and $\mathbf{P}_b(t)$ are the position coordinates of UAV(a) and UAV(b) at time t , which are represented by the coordinates $(x_a(t), y_a(t), z_a(t))$ and $(x_b(t), y_b(t), z_b(t))$ in a coordinate frame, respectively. From Fig. 1, we see that two UAVs will encounter a minimum miss (or separation) distance, $|\mathbf{R}_m(t)|$, at some point in the future and the miss vector $\mathbf{R}_m(t)$ is calculated as follows

$$\mathbf{R}_m(t) = -\mathbf{R}_{los}(t) + \tau \mathbf{V}_{ab}(t) \quad (3)$$

where τ is the time to closest approach. Since the miss vector $\mathbf{R}_m(t)$ and the relative velocity vector $\mathbf{V}_{ab}(t)$ is orthogonal, we have $\mathbf{R}_m(t) \mathbf{V}_{ab}(t) = 0$. Thus, τ is calculated as follows where $v_{ab,x}(t)$, $v_{ab,y}(t)$ and $v_{ab,z}(t)$ are three components of the relative velocity vector $\mathbf{V}_{ab}(t)$ on x , y and z axes at time t , respectively. At the equation (4), as shown at the bottom of the next page, when two UAVs are getting closer, $\tau > 0$, and when two UAVs are getting further, $\tau < 0$. Thus, when $\tau > 0$, we have to check whether there is a chance to have an event of conflict or not. At $\tau > 0$, the magnitude of $\mathbf{R}_m(t)$ is less than the magnitude of $\mathbf{R}_{los}(t)$ i.e. $|\mathbf{R}_m(t)| = |\mathbf{R}_{los}(t)| \sin \psi < |\mathbf{R}_{los}(t)|$, where ψ is the angle between the LOS vector $\mathbf{R}_{los}(t)$ and the relative velocity vector \mathbf{V}_{ab} . If the magnitude $|\mathbf{R}_m(t)|$ is more than r_{safe} , we have $r_{\text{safe}} < |\mathbf{R}_m(t)| < |\mathbf{R}_{los}(t)|$. This implies that the relative distance of two UAVs is always more than the safety radius. Thus, there is not an event of conflict. However, if the magnitude $|\mathbf{R}_m(t)|$ is less than r_{safe} , an event of conflict will possibly occur. The conflict condition is defined as

$$r_{\text{res}} = r_{\text{safe}} - |\mathbf{R}_m(t)| > 0 \quad (5)$$

where r_{res} is the rest region. If $\tau > 0$ and $|\mathbf{R}_m(t)| < r_{\text{safe}}$ (or $r_{\text{res}} > 0$), a potential conflict will occur. Thus, UAVs should begin to perform the avoidance maneuvers.

III. STRATEGY OF IMPLEMENTING COLLISION AVOIDANCE MANEUVERS

To keep the control system implementable in real time, a strategy is used based on the miss distance $|\mathbf{R}_m(t)|$ of two UAVs. From Fig. 1, we can turn the direction of the

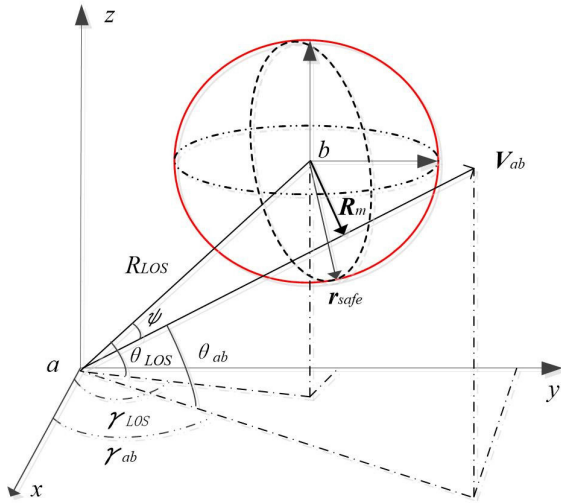


FIGURE 1. Geometric configuration of two UAVs.

relative velocity vector $V_{ab}(t)$ to increase the miss distance $|R_m(t)|$. When this vector's projection line does not intersect the safe sphere but is a tangent to it, $|R_m(t)| = r_{safe}$ and the conflict can be avoided. In general, the direction of the vector $V_{ab}(t)$ is turned towards the direction of the vector $R_m(t)$ to minimize the change of velocity. In the strategy, the avoidance maneuver is implemented by changing the flight direction of UAV(a). This means that UAV(a) is needed to take overall responsibility for avoidance.

At sample time t , let $V_{ab}^*(t)$ represents a new relative velocity vector; $\gamma_{ab}^*(t)$ and $\theta_{ab}^*(t)$ represent the heading and elevation angles of $V_{ab}^*(t)$, respectively. For the sake of clarity and simplicity of notations, the symbol “(t)” on all of time variables is omitted in the following text.

If we adjust only the heading angle of V_a to achieve the desired separation distance r_{safe} between two UAVs, this new relative velocity vector V_{ab}^* should be a tangent to the safety boundary in the horizontal plane. Thus, we have

$$\begin{aligned} |R_m^{H*}| &= |R_{los}| \cos(\theta_{ab} - \theta_{los}) \sin|\gamma_{ab}^* - \gamma_{los}| \\ &= \sqrt{r_{safe}^2 - |R_m^v|^2} \end{aligned} \quad (6)$$

where $|R_{los}|$, γ_{los} and θ_{los} are the magnitude, heading angle and elevation angle of R_{los} , respectively. $|R_m^v|$ is the vertical component of R_m . By rearranging the equation (6), the heading angle of the new relative velocity vector V_{ab}^* is obtained

$$\gamma_{ab}^* = \gamma_{los} \pm \sin^{-1} \frac{\sqrt{r_{safe}^2 - |R_m^v|^2}}{|R_{los}| \cos(\theta_{ab} - \theta_{los})} \quad (7)$$

Similarly, if we adjust only the elevation angle of V_a to make the new relative velocity vector V_{ab}^* to be a tangent to

the safety boundary in the vertical plane, we have

$$|R_m^{v*}| = |R_{los}| \sin|\theta_{ab}^* - \theta_{los}| = \sqrt{r_{safe}^2 - |R_m^H|^2} \quad (8)$$

where $|R_m^H|$ is the horizontal component of R_m . While keeping the heading angle constant, the elevation angle of the new relative velocity vector V_{ab}^* is obtained from the equation (8), i.e.

$$\theta_{ab}^* = \theta_{los} \pm \sin^{-1} \frac{\sqrt{r_{safe}^2 - |R_m^H|^2}}{|R_{los}|} \quad (9)$$

A. THE AVOIDANCE MANEUVER ONLY IN THE HORIZONTAL PLANE

By changing the heading angle γ_a of the UAV(a), the heading angle γ_{ab} of the relative velocity vector V_{ab} can be turned. If we change the heading angle to γ_a^* from γ_a , the heading angle γ_{ab} is turned to γ_{ab}^* . The x and y components of the new relative velocity vector V_{ab}^* can be written as

$$v_{ab,x}^* = |V_b| \cos(\theta_b) \cos(\gamma_b) - |V_a| \cos(\theta_a) \cos(\gamma_a^*) \quad (10)$$

$$v_{ab,y}^* = |V_b| \cos(\theta_b) \sin(\gamma_b) - |V_a| \cos(\theta_a) \sin(\gamma_a^*) \quad (11)$$

Further, we have

$$\begin{aligned} \tan(\gamma_{ab}^*) &= \frac{v_{ab,y}^*}{v_{ab,x}^*} \\ &= \frac{|V_b| \cos(\theta_b) \sin(\gamma_b) - |V_a| \cos(\theta_a) \sin(\gamma_a^*)}{|V_b| \cos(\theta_b) \cos(\gamma_b) - |V_a| \cos(\theta_a) \cos(\gamma_a^*)} \end{aligned} \quad (12)$$

where γ_{ab}^* is given by the equation (7). From (7), we will have a total of 4 solutions for γ_{ab}^* , two due to the nature of the inverse sine function (γ and $\pi - \gamma$) and each of those will have two solution due to \pm sign. In all four solutions, we select one solution to achieve the desired separation distance with the minimum deviation. After some algebraic manipulation of equation (12), we have

$$|V_a| \sin(\gamma_a^* - \gamma_{ab}^*) = |V_b| \frac{\cos(\theta_b)}{\cos(\theta_a)} \sin(\gamma_b - \gamma_{ab}^*) \quad (13)$$

Thus, if $\frac{|V_b| \cos(\theta_b)}{|V_a| \cos(\theta_a)} \sin(\gamma_b - \gamma_{ab}^*) \leq 1$, the heading angle γ_a^* is obtained, i.e.

$$\gamma_a^* = \gamma_{ab}^* + \sin^{-1} \left(\frac{|V_b| \cos(\theta_b)}{|V_a| \cos(\theta_a)} \sin(\gamma_b - \gamma_{ab}^*) \right). \quad (14)$$

$$\tau = \frac{R_{los}(t) \cdot V_{ab}(t)}{V_{ab}(t) \cdot V_{ab}(t)} = - \frac{(x_b(t) - x_a(t))v_{ab,x}(t) + (y_b(t) - y_a(t))v_{ab,y}(t) + (z_b(t) - z_a(t))v_{ab,z}(t)}{v_{ab,x}(t)v_{ab,x}(t) + v_{ab,y}(t)v_{ab,y}(t) + v_{ab,z}(t)v_{ab,z}(t)} \quad (4)$$

B. THE AVOIDANCE MANEUVER ONLY IN THE VERTICAL PLANE

Similarly, if we change the elevation angle to θ_a^* from θ_a , the elevation angle θ_{ab} is turned to θ_{ab}^* . The z component of the new relative velocity vector V_{ab}^* can be written as

$$v_{ab,z}^* = |V_b| \sin(\theta_b) - |V_a| \sin(\theta_a^*) \tag{15}$$

Further, we have

$$\tan(\theta_{ab}^*) = \frac{\sin(\theta_{ab}^*)}{\cos(\theta_{ab}^*)} = \frac{v_{ab,z}^*}{\sqrt{(v_{ab,x}^*)^2 + (v_{ab,z}^*)^2}} \tag{16}$$

where θ_{ab}^* is given by the equation (9). From (9), we will have a total of 2 solutions for θ_{ab}^* , due to \pm sign. In two solutions, we select one solution to achieve the desired separation distance with the minimum deviation. The equations (10), (11) and (15) are substituted into the equation (16). After some algebraic manipulation of the equation (16), we have

$$\begin{aligned} & \left(\frac{|V_a|}{|V_b|}\right)^2 \left(\sin^2(\theta_a^*) - \sin^2(\theta_{ab}^*)\right) \\ & - 2 \left(\frac{|V_a|}{|V_b|}\right) \left(\sin(\theta_a^*) \sin(\theta_b) \cos^2(\theta_{ab}^*)\right) \\ & - \cos(\theta_a^*) \cos(\theta_b) \sin^2(\theta_{ab}^*) \cos(\gamma_a - \gamma_b) \\ & = \left(\sin^2(\theta_{ab}^*) - \sin^2(\theta_b)\right) \end{aligned} \tag{17}$$

The equation (17) is non-linear and can be solved iteratively. According to triangle given by the equation (1), we have $\theta_{max,c} > \theta_a^* > \theta_a$ at $\theta_{ab}^* > \theta_{ab}$ and $\theta_a > \theta_a^* > -\theta_{max,d}$ at $\theta_{ab}^* < \theta_{ab}$, where $\theta_{max,c}$ is the maximum pitch angle in the vertical climb and $\theta_{max,d}$ is the maximum dive angle in the vertical descent. These values are determined by the maneuver parameters of UAV [35].

C. THE AVOIDANCE MANEUVER IN BOTH HORIZONTAL AND VERTICAL PLANE

When the heading-elevation combination change, the equations (13) and (17) are modified as

$$\begin{aligned} & |V_a| \sin(\gamma_a^* - \gamma_{ab}^*) \\ & = |V_b| \frac{\cos(\theta_b)}{\cos(\theta_a^*)} \sin(\gamma_b - \gamma_{ab}^*) \end{aligned} \tag{18a}$$

$$\begin{aligned} & \left(\frac{|V_a|}{|V_b|}\right)^2 \left(\sin^2(\theta_a^*) - \sin^2(\theta_{ab}^*)\right) \\ & - 2 \left(\frac{|V_a|}{|V_b|}\right) \left(\sin(\theta_a^*) \sin(\theta_b) \cos^2(\theta_{ab}^*)\right) \\ & - \cos(\theta_a^*) \cos(\theta_b) \sin^2(\theta_{ab}^*) \cos(\gamma_a - \gamma_b) \\ & = \left(\sin^2(\theta_{ab}^*) - \sin^2(\theta_b)\right) \end{aligned} \tag{18b}$$

The equations (18a) and (18b) are solved simultaneously, so that the heading angle γ_a^* and the elevation angle θ_a^* can be obtained.

D. THE IMPLEMENTATION LOGIC OF THE AVOIDANCE MANEUVER

Since the equation (14) is closed-form formulas, the less time is needed for computing heading angle γ_a^* . But, the equation (17) is only solved iteratively. Thus, the more time is needed for computing elevation angle θ_a^* . For a constant sampling interval, the increase of computational time results in the decrease of time performed the avoidance maneuver. This means that the avoidance maneuver in the horizontal plane begins earlier than that in the vertical plane. In addition, the climb maneuver consumes more power than horizontal maneuver and descent maneuver in low-altitude flights increases the chance of hitting obstacles. For the avoidance maneuver, therefore, priority should be given to the horizontal plane. When $\frac{|V_b| \cos(\theta_b)}{|V_a| \cos(\theta_a)} \sin(\gamma_b - \gamma_{ab}^*) > 1$, however, the heading angle γ_a^* is not obtained. In this case, priority is given to the vertical plane. When the maneuver only in one plane cannot avoid successfully obstacles, the maneuver in both the horizontal and vertical plane is used. But, this means that more computational time is requested for computing heading and elevation angles. Then, the following order is used for selecting the avoidance maneuvers:

- 1) maneuver only in the horizontal plane;
- 2) maneuver only in the vertical plane;
- 3) maneuver in both the horizontal and vertical plane;

Then, the expected heading angle or/and elevation angle of UAV(a) are computed at each sampling time. During time sampling interval, the flight controller of UAV(a) adjusts uniformly the heading angle or/and elevation angle to the expected value in the case that the magnitude of velocity V_a keeps a constant. This proceeding is continuously run at each sampling time, until the avoidance maneuver end, i.e. $|R_m(i)| \geq r_{safe}$. Thus, it is ensured that the separation distance between two UAVs is always larger than the safety radius. Table 1 gives the pseudo code for the implementation logic of the avoidance maneuver at sampling time i . It is noted that the proposed strategy does not constrain that all UAVs have constant ground speeds and direction of the velocity. Thus, it is very suitable in reality application.

In Table 1, $r_{m,x}(i)$; $r_{m,y}(i)$ and $r_{m,z}(i)$ are three components of the minimum separation distance $R_m(i)$ on x , y and z axes at sampling time i .

IV. THE ANALYSIS FOR SUCCESSFUL COLLISION AVOIDANCE

When the velocity vector of all UAVs is constant in the collision avoidance process, the condition for successful avoidance is derived in [23]. However, it is not suitable for the case that the velocity vector is time-varying. This section investigates the effect of time-varying velocity on the collision avoidance.

In order to characterize the behavior of relative velocity vector V_{ab} in a spherical coordinate frame constituting by r , γ and θ axes, we compute three components of V_{ab} in a spherical coordinate frame. As shown in Fig. 2, first rotate

TABLE 1. Pseudo code for the avoidance maneuver.

Input: $r_{m,x}(i)$; $r_{m,y}(i)$ and $r_{m,z}(i)$
 Computing $|\mathbf{R}_m^H| = \sqrt{(r_{m,x}(i))^2 + (r_{m,y}(i))^2}$ and
 $|\mathbf{R}_m^V| = r_{m,z}(i)$
 Computing γ_{ab}^* by the equation (7)
 Computing θ_{ab}^* by the equation (9)
If $\frac{|v_b| \cos(\theta_b)}{|v_a| \cos(\theta_a)} \sin(\gamma_b - \gamma_{ab}^*) \leq 1$
 Computing γ_a^* by the equation (14)
 Let $\theta_a^* = \theta_a$
Else
 Computing θ_a^* by the equation (17)
If $\theta_{max,c} > \theta_a^* > -\theta_{max,d}$
 Let $\gamma_a^* = \gamma_a$
Else
 Computing γ_a^* and θ_a^* by combining the equations (18a)
 and (18b)
End
End
Output: γ_a^* ; θ_a^*

the original frame of reference by $\gamma_{ab}(k)$ about the z axis and then rotate the resulting frame about the new y axis by $\theta_{ab}(k)$. In this new reference frame, the new x , y and z axes are called as r , γ and θ axes, respectively. The component of \mathbf{V}_{ab} along r , γ and θ axes are denoted by $v_{ab,r}$, $v_{ab,\gamma}$ and $v_{ab,\theta}$, respectively. Thus, $v_{ab,r}$ is the component of \mathbf{V}_{ab} along the distance vector \mathbf{r}_{ac} and the $v_{ab,\gamma}$ and $v_{ab,\theta}$ represents the component normal to the distance vector \mathbf{r}_{ac} , where the direction of the distance vector \mathbf{r}_{ac} is identical with the direction of the relative velocity vector $\mathbf{V}_{ab}(k)$. Obviously, they satisfy $v_{ab,r}(k) = |\mathbf{V}_{ab}(k)|$, $v_{ab,\gamma}(k) = 0$ and $v_{ab,\theta}(k) = 0$. When $t \in (k, k + t_{sam}]$ (where t_{sam} is the sampling time interval), three components of \mathbf{V}_{ab} in a spherical coordinate frame can be obtained by the rotational transformations described above [4],

$$v_{ab,r}(t) = |\mathbf{V}_b(t)| [\cos(\theta_b(t)) \cos(\theta_{ab}(k)) \cos(\gamma_b(t) - \gamma_{ab}(k)) + \sin(\theta_b(t)) \sin(\theta_{ab}(k))] - |\mathbf{V}_a(t)| [\cos(\theta_a(t)) \cos(\theta_{ab}(k)) \cos(\gamma_a(t) - \gamma_{ab}(k)) + \sin(\theta_a(t)) \sin(\theta_{ab}(k))] \quad (19a)$$

$$v_{ab,\gamma}(t) = |\mathbf{V}_b(t)| \cos(\theta_b(t)) \sin(\gamma_b(t) - \gamma_{ab}(k)) - |\mathbf{V}_a(t)| \cos(\theta_a(t)) \sin(\gamma_a(t) - \gamma_{ab}(k)) \quad (19b)$$

$$v_{ab,\theta}(t) = |\mathbf{V}_b(t)| [-\cos(\theta_b(t)) \sin(\theta_{ab}(k)) \cos(\gamma_b(t) - \gamma_{ab}(k)) + \sin(\theta_b(t)) \cos(\theta_{ab}(k))] - |\mathbf{V}_a(t)| [-\cos(\theta_a(t)) \sin(\theta_{ab}(k)) \cos(\gamma_a(t) - \gamma_{ab}(k)) + \sin(\theta_a(t)) \cos(\theta_{ab}(k))] \quad (19c)$$

And there is following relation.

$$v_{ab,r}^2(t) + v_{ab,\gamma}^2(t) + v_{ab,\theta}^2(t) = |\mathbf{V}_{ab}(t)|^2 \quad (20)$$

Using the sensor measurements obtained in sampling time k , the heading angle $\gamma_{ab}(k)$ and the elevation angle $\theta_{ab}(k)$

TABLE 2. Eight cases for increasing ψ .

$v_{ab,\gamma}(t)$	$v_{ab,\theta}(t)$	$\gamma_{ab}(k)$	$\theta_{ab}(k)$
> 0	$= 0$	$> \gamma_{los}$	arbitrary
< 0	$= 0$	$< \gamma_{los}$	arbitrary
$= 0$	> 0	arbitrary	$> \theta_{los}$
$= 0$	< 0	arbitrary	$< \theta_{los}$
> 0	> 0	$> \gamma_{los}$	$> \theta_{los}$
> 0	< 0	$> \gamma_{los}$	$< \theta_{los}$
< 0	> 0	$< \gamma_{los}$	$> \theta_{los}$
< 0	< 0	$< \gamma_{los}$	$< \theta_{los}$

of the relative velocity vector $\mathbf{V}_{ab}(k)$ can be obtained by the equations (12) and (16).

If $v_{ab,\gamma}(t) \neq 0$ or/and $v_{ab,\theta}(t) \neq 0$, the angle ψ between $\mathbf{R}_{los}(t)$ and $\mathbf{V}_{ab}(t)$ increases in eight cases given by Table 2. In other words, the relative velocity vector $\mathbf{V}_{ab}(t)$ is turned towards the outside of safety sphere, as shown in Fig. 2(a). For these cases, if $|\mathbf{R}_m(k)| < r_{safe}$, a scalar function is defined as

$$y(t) = \tau_k |\mathbf{V}_{ab}(k)| - \sqrt{r_{safe}^2 - |\mathbf{R}_m(k)|^2} - \int_k^t v_{ab,r}(t) dt \quad (21a)$$

where $t \in (k, k + t_{sam}]$.

Besides above eight cases, the angle ψ between $\mathbf{R}_{los}(t)$ and $\mathbf{V}_{ab}(t)$ decreases. In other words, the relative velocity vector $\mathbf{V}_{ab}(t)$ is towards the inside of safety sphere, as shown in Fig. 2(b). For this case, the scalar function is redefined as

$$y(t) = \tau_k |\mathbf{V}_{ab}(k)| - r_{safe} - \int_k^t v_{ab,r}(t) dt \quad (21b)$$

If $y(t) \geq 0$, no collision between two UAVs will occur. Thus, the successful collision avoidance is guaranteed at $t \in (k, k + t_{sam}]$.

Since the avoidance maneuvers are implemented by changing the heading angle $\gamma_a(t)$ or/and the elevation angle $\theta_a(t)$ of the velocity vector $\mathbf{V}_a(t)$, the relative velocity vector $\mathbf{V}_{ab}(t)$ is time-varying. In addition, the change of the velocity vector $\mathbf{V}_b(t)$, which is unknown in advance, can also cause the change of the relative velocity vector $\mathbf{V}_{ab}(t)$. Since $\int_k^t v_{ab,r}(t) dt < \int_k^{k+t_{sam}} v_{ab,r}(t) dt$ at $v_{ab,r}(t) > 0$, we have $y(t) \geq y(k + t_{sam})$. When the relative velocity vector $\mathbf{V}_{ab}(t)$ is turned towards the outside of safety sphere, the condition required for successful collision avoidance is given by

$$\tau_k |\mathbf{V}_{ab}(k)| - \sqrt{r_{safe}^2 - |\mathbf{R}_m(k)|^2} - \int_k^{k+t_{sam}} v_{ab,r}(t) dt > 0 \quad (22a)$$

This condition is suitable only in the case that $|\mathbf{R}_m(k)| < r_{safe}$ and $t \in (k, k + t_{sam}]$. If the relative velocity vector $\mathbf{V}_{ab}(t)$

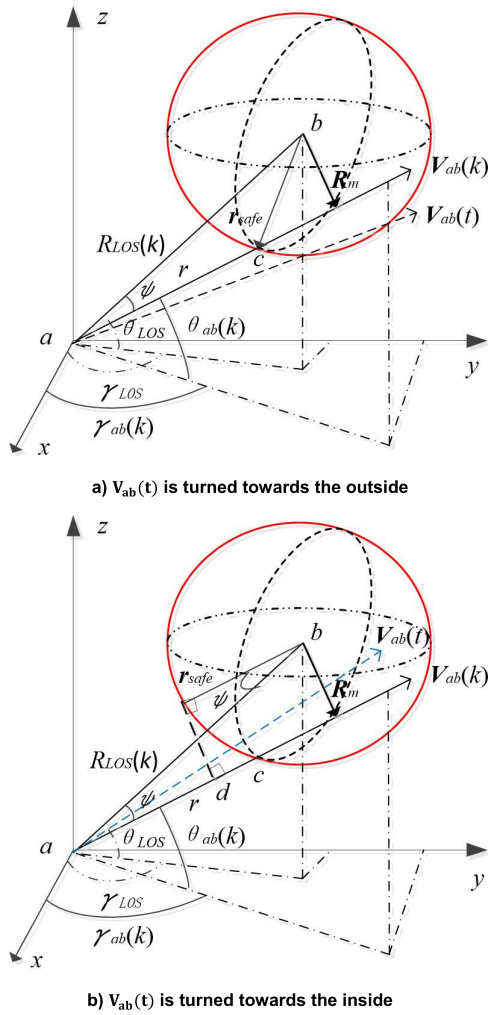


FIGURE 2. The analysis for successful avoidance.

is turned towards the inside of safety sphere, this condition becomes as

$$\tau_k |\mathbf{V}_{ab}(k)| - r_{\text{safe}} - \int_k^{k+t_{\text{sam}}} v_{ab,r}(t) dt > 0 \quad (22b)$$

where $v_{ab,r}(t)$ is unknown, but it is estimated in advance. Using the condition given by (22a) or (22b), thus, we can forecast whether the successful collision avoidance is achieved during $t \in (k, k + t_{\text{sam}}]$. The UAV flight paths may include loiter patterns, search patterns, traffic patterns and various turning maneuvers [22]. For these different patterns, $\mathbf{V}_{ab}(t)$ changes at different forms. For various $\mathbf{V}_{ab}(t)$, the conditions required for successful collision avoidance are discussed as following.

1) $|\mathbf{V}_{ab}(t)|$ keeps constant, i.e. $|\mathbf{V}_{ab}(t)| = |\mathbf{V}_{ab}(k)|$, such as loiter patterns and turning maneuver. In this case, $v_{ab,r}(t) < |\mathbf{V}_{ab}(k)|$ due to

$$v_{ab,r}(t) = \sqrt{|\mathbf{V}_{ab}(k)|^2 - v_{ab,\gamma}^2(t) - v_{ab,\theta}^2(t)}$$

Thus, $\int_k^{k+t_{\text{sam}}} v_{ab,r}(t) dt < \int_k^{k+t_{\text{sam}}} |\mathbf{V}_{ab}(k)| dt = |\mathbf{V}_{ab}(k)| t_{\text{sam}}$. Further, we have

$$\begin{aligned} y(t) &> y(k + t_{\text{sam}}) \\ &= \tau_k |\mathbf{V}_{ab}(k)| - \sqrt{r_{\text{safe}}^2 - |\mathbf{R}_m(k)|^2} \\ &\quad - \int_k^{k+t_{\text{sam}}} v_{ab,r}(t) dt > \tau_k |\mathbf{V}_{ab}(k)| \\ &\quad - \sqrt{r_{\text{safe}}^2 - |\mathbf{R}_m(k)|^2} - |\mathbf{V}_{ab}(k)| t_{\text{sam}} \quad (23) \end{aligned}$$

At $t \in (k, k + t_{\text{sam}}]$, the condition required for successful collision avoidance becomes as

$$(\tau_k - t_{\text{sam}}) |\mathbf{V}_{ab}(k)| - \sqrt{r_{\text{safe}}^2 - |\mathbf{R}_m(k)|^2} > 0 \quad (24)$$

Similarly, corresponding to the equation (22b), the condition required for successful collision avoidance is

$$(\tau_k - t_{\text{sam}}) |\mathbf{V}_{ab}(k)| - r_{\text{safe}} > 0 \quad (25)$$

In this case, $v_{ab,r}(t)$ don't need to know in advance. Using the information at the sampling time k , we can test whether the successful collision avoidance is achieved at $t \in (k, k + t_{\text{sam}}]$.

2) The derivative of $\mathbf{V}_{ab}(t)$ keeps constant and $v_{ab,\gamma}(t) = 0$, $v_{ab,\theta}(t) = 0$, such as traffic patterns and search patterns. In this case, the direction of $\mathbf{V}_{ab}(t)$ is not varied, i.e. $v_{ab,r}(t) = \mathbf{V}_{ab}(t) = |\mathbf{V}_{ab}(k)| + a(t - k)$, where a is the constant acceleration. From the equation (21a), we have

$$\begin{aligned} y(t) &= \tau_k |\mathbf{V}_{ab}(k)| - \sqrt{r_{\text{safe}}^2 - |\mathbf{R}_m(k)|^2} \\ &\quad - |\mathbf{V}_{ab}(k)| (t - k) - \frac{1}{2} a (t - k)^2 \quad (26) \end{aligned}$$

Since $y(t) > y(k + t_{\text{sam}})$, the condition required for successful collision avoidance is given by

$$(\tau_k - t_{\text{sam}}) |\mathbf{V}_{ab}(k)| - \sqrt{r_{\text{safe}}^2 - |\mathbf{R}_m(k)|^2} - \frac{1}{2} a (t_{\text{sam}})^2 > 0 \quad (27)$$

where a is unknown but estimated by $(|\mathbf{V}_{ab}(k)| - |\mathbf{V}_{ab}(k-1)|)/t_{\text{sam}}$. For successful collision avoidance, the acceleration a must be limited to

$$a < a_{\text{max}} = \frac{2}{(t_{\text{sam}})^2} [(\tau_k - t_{\text{sam}}) |\mathbf{V}_{ab}(k)| - \sqrt{r_{\text{safe}}^2 - |\mathbf{R}_m(k)|^2}] \quad (28)$$

3) The derivative of $v_{ab,r}(t)$ keeps constant and $v_{ab,\gamma}(t) \neq 0$, $v_{ab,\theta}(t) \neq 0$, such as search patterns and turning maneuver. In this case, the direction of $\mathbf{V}_{ab}(t)$ is time-varying and $v_{ab,r}(t) = |\mathbf{V}_{ab}(k)| + a(t - k)$. When the direction of $\mathbf{V}_{ab}(t)$ is turned towards the outside of safety sphere, the condition required for successful collision avoidance is given by the equation (27). If the direction of $\mathbf{V}_{ab}(t)$ is turned towards the inside of safety sphere, the condition required for successful collision avoidance is given by

$$(\tau_k - t_{\text{sam}}) |\mathbf{V}_{ab}(k)| - r_{\text{safe}} - \frac{1}{2} a (t_{\text{sam}})^2 > 0 \quad (29)$$

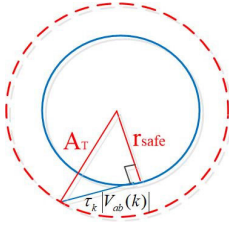


FIGURE 3. The geometric relation for the modify measure.

Similar with second case, the acceleration a must be estimated to test whether the successful collision avoidance is achieved.

The collision avoidance strategy proposed in this paper is that the direction of $\mathbf{V}_{ab}(t)$ is turned towards the outside of safety sphere by changing the heading angle $\gamma_a(t)$ or/and the elevation angle $\theta_a(t)$ of the velocity vector $\mathbf{V}_a(t)$. If the equation (22a) is satisfied in all of the sampling time interval, the collision between UAV(a) and UAV(b) can be avoided successfully. But, the time to closest approach τ decreases along with the decrease of the distance between UAV(a) and UAV(b). When $\tau_k < \sqrt{r_{\text{safe}}^2 - |\mathbf{R}_m(k)|^2} / |\mathbf{V}_{ab}(k)|$ and $|\mathbf{R}_m(k)| < r_{\text{safe}}$, the collision between UAV(a) and UAV(b) may occur at the sampling time k . To prevent complete failure and enhance safety during execution of avoidance maneuver, it is desirable to do modification to the collision avoidance strategy. A simple and feasible modify measure is to define a new alerting threshold A_r . Let $A_r = r_{\text{safe}} + \Delta r$. This implies that the beginning time of the avoidance maneuvers is advanced. Thus, the equation (21a) can be rewritten as

$$y(t) = \tau_k |\mathbf{V}_{ab}(k)| - \sqrt{A_r^2 - |\mathbf{R}_m(k)|^2} - \int_k^t v_{ab,r}(t) dt \quad (30)$$

A constant Δr is selected, so that $r_{\text{safe}} \leq |\mathbf{R}_m(k)| < A_r$ at $\tau_k < \sqrt{A_r^2 - |\mathbf{R}_m(k)|^2} / |\mathbf{V}_{ab}(k)|$. This implies that the distance between two UAVs is more than r_{safe} even though $y(t) < 0$. Thus, the collision avoidance is guaranteed. At the sampling time k , suppose $|\mathbf{R}_{los}(k)| = A_r$ when $|\mathbf{R}_m(k)| = r_{\text{safe}}$ as shown in Fig. 3.

Thus, we have

$$\Delta r = \sqrt{(\tau_k |\mathbf{V}_{ab}(k)|)^2 + r_{\text{safe}}^2} - r_{\text{safe}} = c_r r_{\text{safe}} \quad (31)$$

where $c_r = \sqrt{\frac{(\tau_k |\mathbf{V}_{ab}(k)|)^2}{r_{\text{safe}}^2} + 1} - 1$. Usually, we have $\tau_k |\mathbf{V}_{ab}(k)| \leq r_{\text{safe}}$. Thus, $c_r < 0.414$. In addition, c_r is also estimated based on $\frac{(\tau_k |\mathbf{V}_{ab,max}|)^2}{r_{\text{safe}}^2}$, where $|\mathbf{V}_{ab,max}|$ is the maximum magnitude of the relative velocity. In practice, $\tau_k = (1 \sim 3)t_{sam}$ is usually selected. Thus, Δr can be obtained from the equation (31).

V. THE CASE OF MULTIPLE INTRUDERS (UAVs)

It is assumed that there are multiple intruders (UAVs) within the range of detection for UAV(a). The number of intruders is $I_o > 1$. By the equation (4), we compute τ_i , which is the time to closest approach between UAV(a) and the i th intruder, from

$i = 1$ to $i = I_o$. For all of intruders with $\tau_i > 0$, we compute the rest region $r_{\text{res},i}$ by the equations (3) and (5). To evaluate the conflict urgency, the prioritization of avoidance maneuver can be confirmed by the value of the rest region r_{res} . The larger is r_{res} , the higher the priority of avoidance is. It is noted that the priority order may be updated at each sampling time, as the states of UAVs change over time.

If all of r_{res} are less than 0, no conflict exists for UAV(a). When the value of only one r_{res} is more than 0, UAV(a) has conflict with one intruder. Thus, the strategy proposed in above sections is used in the case of the pair-wise conflict. If the multiple r_{res} are more than 0, UAV(a) has conflict with multiple intruders. Suppose that there are M_o intruders, which have conflict with UAV(a). In this case, the prioritization of avoidance maneuver can be confirmed by the value of the time to closest approach τ . The smaller is τ , the higher the priority of avoidance is. Overall, the priority of avoidance is sorted by the value of r_{res} for the intruders with $\tau_i > 0$ and the priority of avoidance is sorted by the value of τ for the intruders with $r_{\text{res}} > 0$.

In the case that there are M_o intruders with $r_{\text{res}} > 0$, the avoidance algorithm is given by following.

1) For all intruders, the left and right safety boundary angles in the horizontal plane, as shown in Fig. 4(a), are given by

$$\gamma_{ab_i}^f = \gamma_{los,i} + \sin^{-1} \frac{\sqrt{r_{\text{safe}}^2 - |\mathbf{R}_{m,i}^v|^2}}{|\mathbf{R}_{los,i}| \cos(\theta_{ab_i} - \theta_{los,i})} \quad (32a)$$

$$\gamma_{ab_i}^r = \gamma_{los,i} - \sin^{-1} \frac{\sqrt{r_{\text{safe}}^2 - |\mathbf{R}_{m,i}^v|^2}}{|\mathbf{R}_{los,i}| \cos(\theta_{ab_i} - \theta_{los,i})} \quad (32b)$$

The up and down safety boundary angles in the vertical plane, as shown in Fig. 4(b), are given by

$$\theta_{ab_i}^u = \theta_{los,i} + \sin^{-1} \frac{\sqrt{r_{\text{safe}}^2 - |\mathbf{R}_{m,i}^H|^2}}{|\mathbf{R}_{los,i}|} \quad (33a)$$

$$\theta_{ab_i}^d = \theta_{los,i} - \sin^{-1} \frac{\sqrt{r_{\text{safe}}^2 - |\mathbf{R}_{m,i}^H|^2}}{|\mathbf{R}_{los,i}|} \quad (33b)$$

where $i = 1, \dots, M_o$. $|\mathbf{R}_{los,i}|$, $\gamma_{los,i}$ and $\theta_{los,i}$ are the magnitude, heading angle and elevation angle of LOS vector $\mathbf{R}_{los,i}$ between UAV(a) and the i th intruder, respectively. $|\mathbf{R}_{m,i}^H|$ and $|\mathbf{R}_{m,i}^v|$ are the horizontal and vertical components of the minimum separation distance vector $\mathbf{R}_{m,i}$ between UAV(a) and the i th intruder, respectively. The heading angle and the elevation angle of the relative velocity vector \mathbf{V}_{ab_i} between UAV(a) and the i th intruder are obtained by

$$\gamma_{ab_i} = \tan^{-1} \left(\frac{v_{ab_i,y}}{v_{ab_i,x}} \right); \quad \theta_{ab_i} = \tan^{-1} \left(\frac{v_{ab_i,z}}{\sqrt{(v_{ab_i,x})^2 + (v_{ab_i,y})^2}} \right) \quad (34)$$

where $v_{ab_i,x}$, $v_{ab_i,y}$ and $v_{ab_i,z}$ are the x , y and z components of the relative velocity vector \mathbf{V}_{ab_i} .

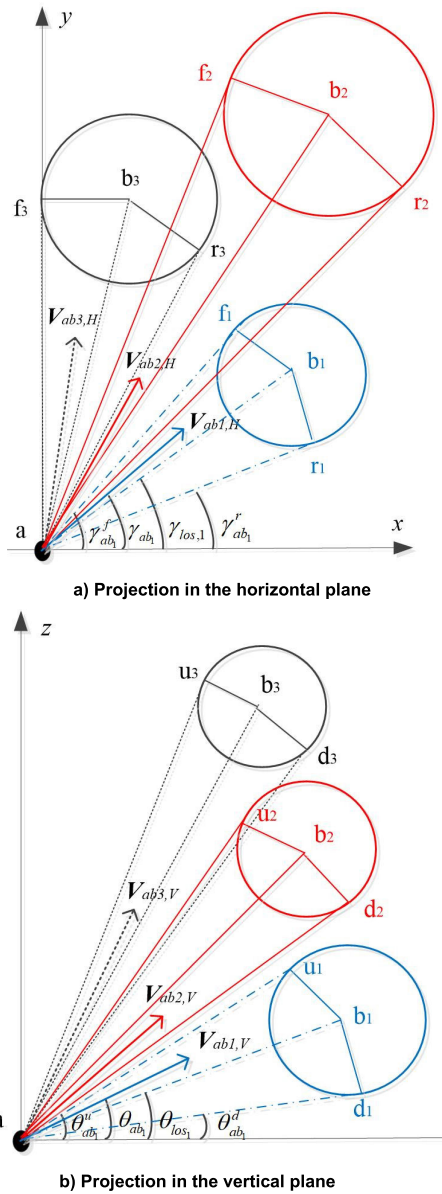


FIGURE 4. Relative Geometry between multiple UAVs.

2) For all of relative velocity vectors, we compute their turning angles to avoid collisions:

$$\sigma_{f,i} = abs(\gamma_{ab_i}^f - \gamma_{ab_i}) \quad (\text{left turning angle}) \quad (35a)$$

$$\sigma_{r,i} = abs(\gamma_{ab_i} - \gamma_{ab_i}^r) \quad (\text{right turning angle}) \quad (35b)$$

$$\sigma_{u,i} = abs(\theta_{ab_i}^u - \theta_{ab_i}) \quad (\text{up turning angle}) \quad (35c)$$

$$\sigma_{d,i} = abs(\theta_{ab_i} - \theta_{ab_i}^d) \quad (\text{down turning angle}) \quad (35d)$$

Then, the maximum left and right tuning angle are obtained by $\sigma_f = \max(\sigma_{f,1}, \dots, \sigma_{f,M_0})$ and $\sigma_r = \max(\sigma_{r,1}, \dots, \sigma_{r,M_0})$. Similarly, the maximum up and down tuning angle are obtained by $\sigma_u = \max(\sigma_{u,1}, \dots, \sigma_{u,M_0})$ and $\sigma_d = \max(\sigma_{d,1}, \dots, \sigma_{d,M_0})$.

3) Let $\tau_i = \min(\tau_1, \dots, \tau_{M_0})$. The new heading angle and new elevation angle of the relative velocity vector V_{ab_i} are

written as

$$\gamma_{ab_i}^* = \gamma_{ab_i} + \sigma_f \quad (\sigma_{f,i} < \sigma_{r,i}) \quad (36a)$$

$$\gamma_{ab_i}^* = \gamma_{ab_i} - \sigma_r \quad (\sigma_{f,i} \geq \sigma_{r,i}) \quad (36b)$$

$$\theta_{ab_i}^* = \theta_{ab_i} + \sigma_u \quad (\sigma_{u,i} < \sigma_{d,i}) \quad (36c)$$

$$\theta_{ab_i}^* = \theta_{ab_i} - \sigma_d \quad (\sigma_{u,i} \geq \sigma_{d,i}) \quad (36d)$$

4) By using the new heading angle of V_{ab_i} , the new heading angle γ_a^* of UAV(a) is obtained by

$$\gamma_a^* = \gamma_{ab_i}^* + \sin^{-1} \left(\frac{|V_{b_i}| \cos(\theta_{b_i})}{|V_a| \cos(\theta_a)} \sin(\gamma_{b_i} - \gamma_{ab_i}^*) \right) \quad (37)$$

where $\frac{|V_{b_i}| \cos(\theta_{b_i})}{|V_a| \cos(\theta_a)} \sin(\gamma_{b_i} - \gamma_{ab_i}^*) \leq 1$. Further, the new elevation angle θ_a^* of UAV(a) is solved by the equation (17).

5) By using the implementation logic of the avoidance maneuver given in the section III-D, the flight controller of UAV(a) adjusts uniformly the heading angle or/and elevation angle to γ_a^* or/and θ_a^* .

VI. STRATEGY OF IMPLEMENTING TRAJECTORY RECOVERY MANEUVERS

After the UAV(a) has finished avoidance maneuver, it is requested to begin a trajectory recovery maneuver at $\tau < 0$. Since the flight trajectory and flight velocity were planned in advance, the aim of trajectory recovery is to make UAV(a) return to the planning trajectory and corresponding planning velocity rapidly. The trajectory recovery strategy proposed in this paper consists of two stages. First stage is that the flight paths lie in bypassed of the safe boundary and second stage is that the flight paths is far from the safe boundary. In each of stage, the flight controller of UAV(a) adjusts the heading angle or elevation angle to implement trajectory recovery maneuvers.

A. FIRST STAGE OF TRAJECTORY RECOVERY MANEUVERS

When the avoidance maneuver closes at the sampling time k , the position of UAV(a) is not on its original planning trajectory, i.e. $P_a(k) \neq OP_a(k)$, where $OP_a(k)$ represents the position of UAV(a) on original planning trajectory. To go back original planning trajectory, the UAV(a) has need of moving from $P_a(k)$ to $OP_a(k)$. However, if the returning path is the straight line, it may intersect the safe boundary sphere. To avoid the returning path intersecting with the safe boundary sphere, UAV(a) must bypass the safe sphere by changing constantly its flight direction. In first stage of trajectory recovery maneuvers, the proposed algorithm is in following:

First, let $(x_g(k), y_g(k), z_g(k))$ is the position coordinates of goal point $OP_a(k)$ and $(x_a(j), y_a(j), z_a(j))$ is the position coordinates of current point $P_a(j)$, where the original time j of the iteration in first stage is equal to the sampling time k .

1) the equation of straight line PO from the point $P_a(j)$ to the point $OP_a(k)$ can be written as

$$\frac{x - x_a(j)}{x_g(k) - x_a(j)} = \frac{y - y_a(j)}{y_g(k) - y_a(j)} = \frac{z - z_a(j)}{z_g(k) - z_a(j)} \quad (38)$$

2) the equation of safe boundary sphere can be written as

$$(x - x_b(j))^2 + (y - y_b(j))^2 + (z - z_b(j))^2 = r_{\text{safe}}^2 \quad (39)$$

where $(x_b(j), y_b(j), z_b(j))$ is the position coordinates of point $P_b(j)$, which is the center of the safe boundary sphere.

3) the equations (38) and (39) are solved simultaneously to obtain the intersecting points between the straight line and the safe sphere. First, we test the number of root by

$$f_r = B^2 - 4AC \quad (40)$$

where

$$\begin{aligned} A &= q^2 + p^2 + 1, \\ B &= 2(q(x_a(j) - x_b(j)) + p(y_a(j) - y_b(j)) \\ &\quad - (q^2 + p^2)z_a(j) - z_b(j)), \\ C &= (x_a(j) - x_b(j) - qz_a(j))^2 + (y_a(j) - y_b(j) - pz_a(j))^2 \\ &\quad + (z_b(j))^2 - r_{\text{safe}}^2 \end{aligned}$$

$$\text{And } q = \frac{x_g(k) - x_a(j)}{z_g(k) - z_a(j)}, p = \frac{y_g(k) - y_a(j)}{z_g(k) - z_a(j)}.$$

4) If $f_r < 0$, the number of root is equal to 0. In this case, the straight line PO does not intersect the safe boundary sphere, so that there is no collision risk in the returning path. Thus, first stage of trajectory recovery maneuvers closes.

If $f_r = 0$, the number of root is equal to 1. In this case, the straight line PO has one intersecting point with the safe boundary sphere. This means that the straight line PO is tangential with the safe boundary sphere. Thus, the azimuth and the elevation angles of the straight line vector PO are obtained by

$$\gamma_{po} = \tan^{-1} \left(\frac{y_g(k) - y_a(j)}{x_g(k) - x_a(j)} \right) \quad (41a)$$

$$\theta_{po} = \tan^{-1} \left(\frac{z_g(k) - z_a(j)}{\sqrt{(x_g(k) - x_a(j))^2 + (y_g(k) - y_a(j))^2}} \right) \quad (41b)$$

In order to make that the direction of the new relative velocity vector V_{ab}^* is parallel with the vector PO , let $\gamma_{ab}^* = \gamma_{po}$ and $\theta_{ab}^* = \theta_{po}$. Thus, we obtain the new relative velocity vector V_{ab}^* being tangential with the safe boundary sphere. Then, we continue to do next step.

If $f_r > 0$, the number of root is equal to 2. In this case, the straight line PO has two intersecting point with the safe boundary sphere. The position coordinates of two intersecting point $S_{1,2}$ can be obtained by

$$\begin{aligned} x_{1,2}^s &= q(z_{1,2}^s - z_a(j)) + x_a(j) \\ y_{1,2}^s &= p(z_{1,2}^s - z_a(j)) + y_a(j) \\ z_{1,2}^s &= (-B \pm \sqrt{f_r})/2A \end{aligned} \quad (42)$$

Then, we compare the distance from the point $P_a(j)$ to two roots $S_{1,2}$ and select one root with less distance as a boundary point denoted by S . In this case, the straight line PO is not tangential with the safe boundary sphere. Thus, we connect the boundary point S and the center point $P_b(j)$ of the safe

boundary sphere to form a straight line SP . The azimuth and elevation angles of the straight line SP are obtained by

$$\begin{aligned} \gamma_{sp} &= \tan^{-1} \left(\frac{y_b(j) - y^s}{x_b(j) - x^s} \right) \\ \theta_{sp} &= \tan^{-1} \left(\frac{z_b(j) - z^s}{\sqrt{(x_b(j) - x^s)^2 + (y_b(j) - y^s)^2}} \right) \end{aligned} \quad (43)$$

Let

$$\gamma_{ab}^* = \gamma_{sp} - \pi/2 \quad (\gamma_{sp} \geq 0) \quad (44a)$$

$$\gamma_{ab}^* = \gamma_{sp} + \pi/2 \quad (\gamma_{sp} < 0) \quad (44b)$$

And

$$\theta_{ab}^* = \theta_{sp} - \pi/2 \quad (\theta_{sp} \geq 0) \quad (45a)$$

$$\theta_{ab}^* = \theta_{sp} + \pi/2 \quad (\theta_{sp} < 0) \quad (45b)$$

This means that the direction of the new relative velocity vector V_{ab}^* is vertical with the straight line SP . Thus, we obtain the new relative velocity vector V_{ab}^* being tangential with the safe boundary sphere. Then, we continue to do next step.

5) By changing the heading angle γ_a or the elevation angle θ_a of UAV(a), the direction of the relative velocity vector is changed to the expected direction, If $\frac{|V_b| \cos(\theta_b)}{|V_a| \cos(\theta_a)} \sin(\gamma_b - \gamma_{ab}^*) \leq 1$, we change only the heading angle γ_a to γ_a^* but keeping the elevation angle θ_a unvarying, where the heading angle γ_a^* is given by the equation (14). Otherwise, we change only the elevation angle θ_a to θ_a^* but keeping the heading angle γ_a constant, where the elevation angle θ_a^* is given by the equation (17).

6) return to step 1. At next sampling time $j = j + 1$, this process is repeated.

B. SECOND STAGE OF TRAJECTORY RECOVERY MANEUVERS

When first stage of trajectory recovery maneuvers closes at sampling time m , the flight path returning to original planning trajectory do not intersect the safe boundary sphere. Thus, we can adjust the heading and elevation angle of UAV(a) to ensure it going back to the planning trajectory rapidly and recovering the planning velocity. The second stage of trajectory recovery maneuvers consists of three steps.

1) select a suitable goal point. In order to ensure the implementation of simple and reliable maneuvers, a suitable goal point must satisfy two constraints: a) the selected goal point is ahead of flight direction; b) the distance between the selected goal point and the current position point $P_a(m)$ is minimum. In all of sampling points, thus, we select those points satisfied first constraint as the candidates of new goal point. In all of candidate points, then, the point satisfied second constraint is selected as the new goal point OP_a .

2) approach the new goal point. First, we compute the azimuth angle (γ_{po}^*) and elevation angle (θ_{po}^*) of the straight line from the current position point $P_a(m)$ to the new goal point OP_a . Then, the heading and elevation angle of UAV(a) are changed to γ_a^* and

θ_a^* , where $\gamma_a^* = \gamma_{po}^*$ and $\theta_a^* = \theta_{po}^*$. At subsequent sampling times, we compute the time of arriving the new goal point. Until that the arriving time is less than one sampling interval, second step closes and return to third step.

3) change the direction of velocity vector. For UAV(a), we change the heading and elevation angle of V_a to γ_o^* and θ_o^* , which are the heading and elevation angles of planning velocity at the new goal point OP_a . Soon after, the trajectory recovery maneuvers have finished. UAV(a) goes back the original planning trajectory.

Table 3 gives the pseudo code for the implementation logic of the trajectory recovery maneuvers.

VII. APPLICATION TO THE FIXED-WING UAV

The 3-D point-mass model of the fixed-wing UAV is derived as following: [9], [14]

$$\dot{x} = |V| \cos \theta \cos \gamma = V_H \cos \gamma \quad (46a)$$

$$\dot{y} = |V| \cos \theta \sin \gamma = V_H \sin \gamma \quad (46b)$$

$$\dot{z} = |V| \sin \theta = V_V \quad (46c)$$

$$\dot{\gamma} = \frac{g \tan \phi}{V_H} \quad |V| = \sqrt{(V_H)^2 + (V_V)^2} \quad (46d)$$

where γ, θ and ϕ denote the heading angle, elevation angle and bank angle of UAV, respectively; g denotes the gravitational acceleration. For the dynamic horizontal turning motion, the maximum horizontal turning rate is given by [35]

$$\dot{\gamma}_{max} = \frac{g}{V_H} \sqrt{(g_{limit})^2 - 1} \quad (47)$$

where g_{limit} is maximum load factor of the UAV. Similar the horizontal maneuvers, there is a maximum turning rate associated with climb or descend maneuver in vertical place, which is given by [35]

$$\dot{\theta}_{max} = \frac{g}{V_V} (g_{limit} - 1) \quad (48)$$

From (47) and (48), g_{limit} limits the rate of changing the heading angle horizontally and the elevation angle vertically. It is noted that g_{limit} has different value for Level Turn, Climb and Descent of airplanes.

To generate the horizontal maneuver, bank command is given as an input, and elevation command is given to generate a vertical maneuver. The dynamic model for θ and ϕ are given as following:

$$\dot{\phi} = \frac{1}{T_\phi} (\phi_{com} - \phi) \quad (49a)$$

$$\dot{\theta} = \frac{1}{T_\theta} (\theta_{com} - \theta) \quad (49b)$$

where T_ϕ and T_θ are the time constant for both dynamics; ϕ_{com} and θ_{com} are the desired value of ϕ and θ in the horizontal and vertical maneuvers. In the case of given the horizontal turning rate $\dot{\gamma}$ and the horizontal flight speed V_H , ϕ_{com} can be obtained from the equation (46d), i.e.

$$\phi_{com} = \tan^{-1} \left(\frac{\dot{\gamma} V_H}{g} \right) \quad (50)$$

TABLE 3. Pseudo code for the trajectory recovery maneuvers.

```

Input:  $P_b(j), P_a(j), V_a(j)$  and  $OP_a(n), (n = k, k + 1, \dots, N)$ 
Let  $\gamma_a^* = \gamma_a$  and  $\theta_a^* = \theta_a$ 
If TRM-sign == 1
  Computing  $f_r$  by the equation (40)
  If  $f_r == 0$ 
    Computing  $\gamma_{po}^*; \theta_{po}^*$  by the equation (41)
    Let  $\gamma_{ab}^* = \gamma_{po}^*$  and  $\theta_{ab}^* = \theta_{po}^*$ 
  End
  If  $f_r > 0$ 
    Computing  $\gamma_{sp}; \theta_{sp}$  by the equation (42) and (43)
    Computing  $\gamma_{ab}^*; \theta_{ab}^*$  by the equation (44) and (45)
  End
  If  $f_r < 0$ 
    Let TRM-sign = 2
  Else
    If  $\frac{|V_b| \cos(\theta_b)}{|V_a| \cos(\theta_a)} \sin(\gamma_b - \gamma_{ab}^*) \leq 1$ 
      Computing  $\gamma_a^*$  by the equation (14)
      Let  $\theta_a^* = \theta_a$ 
    Else
      Computing  $\theta_a^*$  by the equation (17)
      Let  $\gamma_a^* = \gamma_a$ 
    End
  End
If TRM-sign == 2
  For  $n = k: 1: N$ 
    If  $[(x_g(n) - x_a(j))/v_{a,x}(j)] > 0 \ \&\& \ [(y_g(n) - y_a(j))/v_{a,y}(j)] > 0 \ \&\& \ [(z_g(n) - z_a(j))/v_{a,z}(j)] > 0$ 
      Computing
       $d_n = \sqrt{(x_g(n) - x_a(j))^2 + (y_g(n) - y_a(j))^2 + (z_g(n) - z_a(j))^2}$ 
      Add a pair of  $(n, d_n)$  into the 2-D candidate set
    End
  End
  If isempty( $D_g$ ) == 0
    [ $d_{min}, I$ ] = Min( $D_g(:, 2)$ )
    Let the point  $OP_a(I)$  corresponding with  $d_{min}$  as the goal point  $OP_a$ 
     $\gamma_{po} = \tan^{-1} \frac{(y_g(I) - y_a(j))}{(x_g(I) - x_a(j))}$ 
     $\theta_{po} = \tan^{-1} \frac{(z_g(I) - z_a(j))}{\sqrt{(x_g(I) - x_a(j))^2 + (y_g(I) - y_a(j))^2}}$ 
    Let  $\gamma_a^* = \gamma_{po}$ 
    Let  $\theta_a^* = \theta_{po}$ 
    Let TRM-sign = 3
  Else
    If  $[(x_g(k) - x_a(j))/v_{a,x}(j)] > 0 \ \&\& \ [(y_g(k) - y_a(j))/v_{a,y}(j)] > 0$ 
       $\theta_{po} = \tan^{-1} \frac{(z_g(k) - z_a(j))}{\sqrt{(x_g(k) - x_a(j))^2 + (y_g(k) - y_a(j))^2}}$ 
      Let  $\theta_a^* = \theta_{po}$ 

```

When the proposed strategy for the collision avoidance and trajectory recovery is applied to the Fixed-Wing UAVs, the pseudo code of the implementation logic is given in Table 4.

TABLE 3. (Continued.) Pseudo code for the trajectory recovery maneuvers.

```

Else
     $\gamma_{po} = \tan^{-1} \frac{(y_g(k) - y_a(j))}{(x_g(k) - x_a(j))}$ 
    Let  $\gamma_a^* = \gamma_{po}$ 
End
End
End
If TRM-sign == 3
     $t = \frac{\sqrt{(x_g(l) - x_a(j))^2 + (y_g(l) - y_a(j))^2 + (z_g(l) - z_a(j))^2}}{\sqrt{(v_{a,x}(j))^2 + (v_{a,y}(j))^2 + (v_{a,z}(j))^2}}$ 
    If  $t < t_{sam}$ 
        Let TRM-sign = 4
    End
End
If TRM-sign == 4
    If  $|\gamma_o^* - \gamma_a| > 0 \ \&\& \ |\theta_o^* - \theta_a| > 0$ 
        Let  $\gamma_a^* = \gamma_o^*$ 
        Let  $\theta_a^* = \theta_o^*$ 
    Else
        TRM-sign = 1
    End
End
Output:  $\gamma_a^*$  ;  $\theta_a^*$ 

```

VIII. NUMERICAL SIMULATION

A. SIMULATION CONDITIONS

In order to test the performance of the proposed strategy, numerical simulations are performed in seven cases. In the case 1, 2, 3 and 7, two UAVs are in an encounter with each other. In the case 4, 5 and 6, the collision avoidance for multiple UAVs is implemented by using maneuvers only in the horizontal plane, only in the vertical plane, in both horizontal and vertical planes, respectively. In all simulations, the initial simulation conditions are listed in Table 5-7.

In the case 1, 2, 3 and 7, the safe boundary radius is $r_{safe} = 556 \text{ m}$. However, $r_{safe} = 450 \text{ m}$ in the case 4, 5 and 6. From the case 1 to case 5, it is set that constant coefficient $c_r = 0.01$. However, $c_r = 0.04$ for the case 6 and $c_r = 0$ for the case 7. For UAV(a), the maximum horizontal turning rate and the maximum vertical turning rate are set as $\dot{\gamma}_{max} = 10^\circ/s$ and $\dot{\theta}_{max} = 15^\circ/s$, respectively. The range of ϕ_{com} and θ_{com} are set as $[-45^\circ \sim 45^\circ]$ and $[-30^\circ \sim 30^\circ]$, respectively. The sampling time interval $t_{sam} = 1 \text{ s}$.

B. CASE 1

In Case 1, UAV(a) is flight in spiral paths and UAV(b) is flight in straight paths. The initial heading angles of UAV(a) and UAV(b) is opposite in direction. In the horizontal plane, UAV(a) turns right at a constant turning rate. The speed of UAV(b) is varied and the unknown acceleration is equal to $2 \cos(\pi t/60)$. The collision of UAV(a) and UAV(b) will occur in 30 seconds. Fig. 5(a) and 5(b) show the flight paths of collision avoidance and trajectory recovery in 3-D and

TABLE 4. Pseudo code for the proposed strategy.

```

Initialization of parameters
Input:  $V_a(t)$  and  $V_b(t)$ ;  $P_a(t)$  and  $P_b(t)$  at sampling time  $t$ 
    Computing  $V_{ab}(t)$  by the equation (1)
    Computing  $R_{los}(t)$  by the equation (2)
    Computing  $\tau$  by the equation (4)
    If  $\tau \geq 0$ 
        Let TRM-sign = 1
        Computing  $R_m(t)$  by the equation (3)
        Computing  $r_{res} = A_t - |R_m(t)|$ 
        If  $r_{res} \geq 0$ 
            Beginning avoidance maneuver (Table I)
            Computing  $\dot{\gamma} = (\gamma_a^* - \gamma_a)/t_{sam}$ 
            Computing  $\phi_{com}$  by the equation (50)
            Let  $\theta_{com} = \theta_a^*$ 
            Inputting  $\phi_{com}$  and  $\theta_{com}$  to the controller
        End
    Else
        If  $P_a(t) \neq OP_a(t)$ 
            Beginning trajectory recovery maneuver (Table III)
            Computing  $\dot{\gamma} = (\gamma_a^* - \gamma_a)/t_{sam}$ 
            Computing  $\phi_{com}$  by the equation (50)
            Let  $\theta_{com} = \theta_a^*$ 
            Inputting  $\phi_{com}$  and  $\theta_{com}$  to the controller
        End
    End
End
Return to Input at next sampling time  $t = t + t_{sam}$ 

```

2-D plane. Fig. 5(c) shows the relative distance between UAV(a) and UAV(b). Fig. 5(d) gives the command of bank and elevation angle in whole procedure, which are inputs of UAV(a)'s flight controller. From Fig. 5(a) and 5(b), the collision is successfully avoided by adjusting the heading angle of UAV(a). After the collision avoidance, UAV(a) returns to the planning paths by adjusting the heading and elevation angle. From Fig. 5(c), the relative distance is more than the safe radius r_{safe} in whole procedure. The closest distance d_{min} is reached at 27 seconds. The distance difference ($d_{min} - r_{safe}$) between the closest distance and the safe radius is equal to 46.2 m. From Fig. 5(d), all of commands are in the constraint range. In this scenario, the time expended by the collision avoidance and the trajectory recovery is 20 s and 33 s, respectively.

C. CASE 2

In Case 2, UAV(a) and UAV(b) are flight in spiral paths. The initial heading angles of UAV(a) and UAV(b) is cross in direction. In the horizontal plane, UAV(a) and UAV(b) turn right at a constant turning rate. The collision of UAV(a) and UAV(b) will occur in 30 seconds. Fig. 6(a) and 6(b) show the flight paths of collision avoidance and trajectory recovery in 3-D and 2-D plane. Fig. 6(c) shows the relative distance between UAV(a) and UAV(b). Fig. 6(d) gives the command of bank and elevation angle in whole procedure.

TABLE 5. Initial information of UAV(a).

UAV(a)	Case 1, 2, 3	Case 4	Case 5	Case 6	Case 7
Position (m)	(-983.1, 0, 50)	(50, 1544.3, 100)	(2165.1, 0, 90)	(-2162.1, 0, 100)	(-983.1, 0, 50)
Speed (m/s)	(0, 51.5, 5)	(0, -51.5, 0)	(-51.5, 0, 0)	(0, 51.5, 5)	(0, 51.5, 0)
Acceleration (m/s ²)	0	0	0	0	0
Heading angle (rad)	$\pi/2$	$-\pi/2$	π	$\pi/2$	$\pi/2$
Heading angle rate (rad/s)	0.0523	0	0	0.0238	0.0523
Elevation angle (rad)	0.0968	0	0	0	0.0968
Elevation angle rate (rad/s)	0	0	0	0	0

TABLE 6. Initial information of UAV(b) in cases 1, 2, 3 and 7.

UAV(b)	Case 1	Case 2	Case 3	Case 7
Position (m)	(0, 3165.6, 50)	(-983.1, 1966.2, 50)	(983.1, 1966.2, 50)	(0, 3165.6, 50)
Speed (m/s)	(0, -51.5, 5)	(51.5, 0, 5)	(0, -51.5, 5)	(0, -51.5, 0)
Acceleration (m/s ²)	(0, -2, 0)	(0, 0, 0)	(0, 0, 0)	(0, -2, 0)
Heading angle (rad)	$-\pi/2$	0	$\pi/2$	$-\pi/2$
Heading angle rate (rad/s)	0	0.0523	-0.0523	0
Elevation angle (rad)	0.0968	0.0968	0.0968	0.0968
Elevation angle rate (rad/s)	0	0	0	0

TABLE 7. Initial information of UAV(b) in cases 4, 5 and 6.

	UAV(b ₁)	UAV(b ₂)	UAV(b ₃)
Position (m)	(0, -1735.3, 90)	(779.4, -2185.3, 90)	(-779.4, -2185.3, 90)
Speed (m/s)	(0, 51.5, 0.5)	(0, 51.5, 0.5)	(0, 51.5, 0.5)
Acceleration (m/s ²)	(0, 2, 0)	(0, 2, 0)	(0, 2, 0)
Heading angle (rad)	$\pi/2$	$\pi/2$	$\pi/2$
Heading angle rate (rad/s)	0	0	0
Elevation angle (rad)	0.0097	0.0097	0.0097
Elevation angle rate (rad/s)	0	0	0

TABLE 8. The distance difference for different r_{safe} and c_r (unit: m).

r_{safe} (m)	185.32	370.64	555.96	741.28	926.60
$c_r = 0.01$	-2.12	-0.02	2.07	3.70	5.08
$c_r = 0.03$	1.54	7.06	12.63	18.02	23.85

From Fig. 6(a) and 6(b), the collision is successfully avoided by adjusting the heading angle of UAV(a). After the collision avoidance, UAV(a) returns to the planning paths by adjusting the heading and elevation angle. From Fig. 6(c), the relative distance is more than the safe radius r_{safe} in whole procedure. The closest distance d_{min} is reached at 25 seconds. The distance difference ($d_{min} - r_{safe}$) is equal to 2.0 m. For different r_{safe} and c_r , the distance difference ($d_{min} - r_{safe}$) is given by Table 8. From Table 8, the distance difference increases along the increase of r_{safe} and c_r . It is noted that for less r_{safe} , larger c_r should be selected to ensure successful collision avoidance.

From Fig. 6(d), all of commands are in the constraint range. In this scenario, the time expended by the collision avoidance and the trajectory recovery is 12 s and 42 s, respectively.

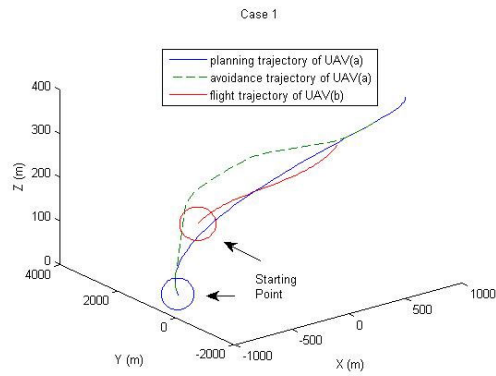
D. CASE 3

In Case 3, UAV(a) and UAV(b) are flight in spiral paths. The initial heading angles of UAV(a) and UAV(b) is opposite

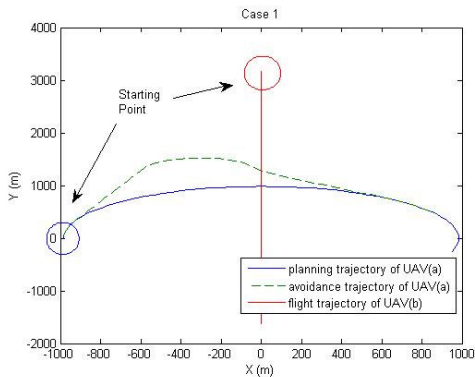
in direction. In the horizontal plane, UAV(a) and UAV(b) turn right at a constant turning rate. The collision of UAV(a) and UAV(b) will occur in 30 seconds. Fig. 7(a) and 7(b) show the flight paths of collision avoidance and trajectory recovery in 3-D and 2-D plane. Fig. 7(c) shows the relative distance between UAV(a) and UAV(b). Fig. 7(d) gives the command of bank and elevation angle in whole procedure. From Fig. 7(a) and 7(b), the collision is successfully avoided by adjusting the heading angle of UAV(a). After the collision avoidance, UAV(a) returns to the planning paths by adjusting the heading and elevation angle. From Fig. 7(c), the relative distance is more than the safe radius r_{safe} in whole procedure. The closest distance d_{min} is reached at 30 seconds. The distance difference ($d_{min} - r_{safe}$) is equal to 3.7 m. From Fig. 7(d), all of commands are in the constraint range. In this scenario, the time expended by the collision avoidance and the trajectory recovery is 14 s and 38 s, respectively.

E. CASE 4

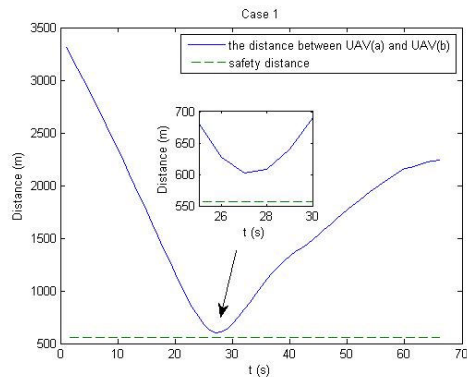
In Case 4, UAV(a) and three intruders (UAV(b₁), UAV(b₂), UAV(b₃)) in formation flight are flight along straight paths. The initial heading angles of UAV(a) and three intruders is opposite in direction. The speed of three intruders is varied and the unknown acceleration is equal to $2 \cos(\pi t/60)$. Fig. 8(a) and 8(b) show the flight paths of collision avoidance



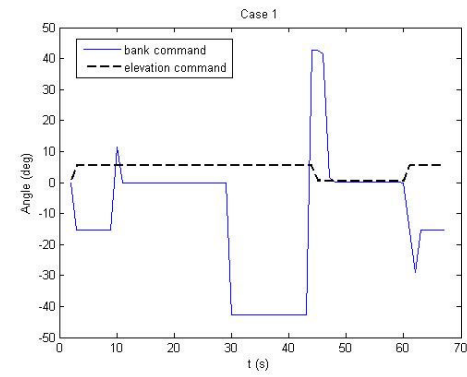
(a) trajectory of two UAVs in 3-D space



(b) trajectory of two UAVs in x-y plane



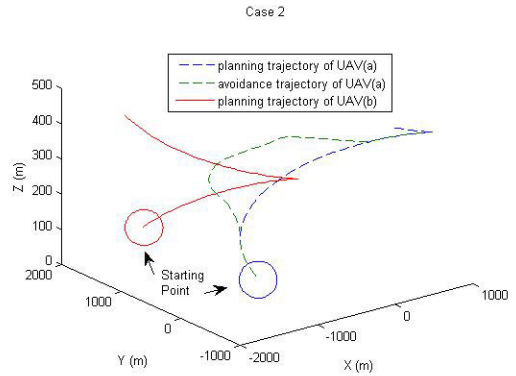
(c) the distance between two UAVs



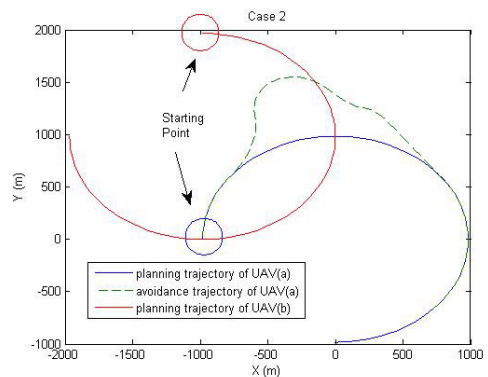
(d) the command of bank and elevation angle

FIGURE 5. Collision avoidance and trajectory recovery in the case 1.

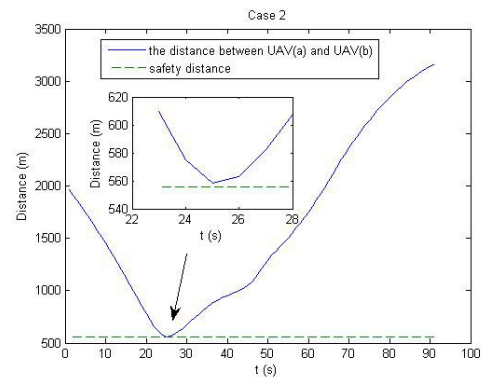
and trajectory recovery in 3-D and 2-D plane. Fig. 8(c) shows the relative distance between UAV(a) and three intruders.



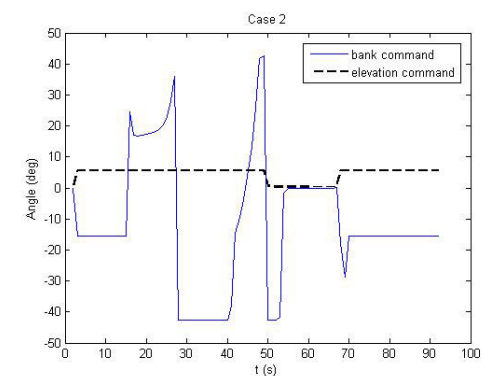
(a) trajectory of two UAVs in 3-D space



(b) trajectory of two UAVs in x-y plane



(c) the distance between two UAVs



(d) the command of bank and elevation angle

FIGURE 6. Collision avoidance and trajectory recovery in the case 2.

Fig. 8(d) gives the command of bank and elevation angle in whole procedure.

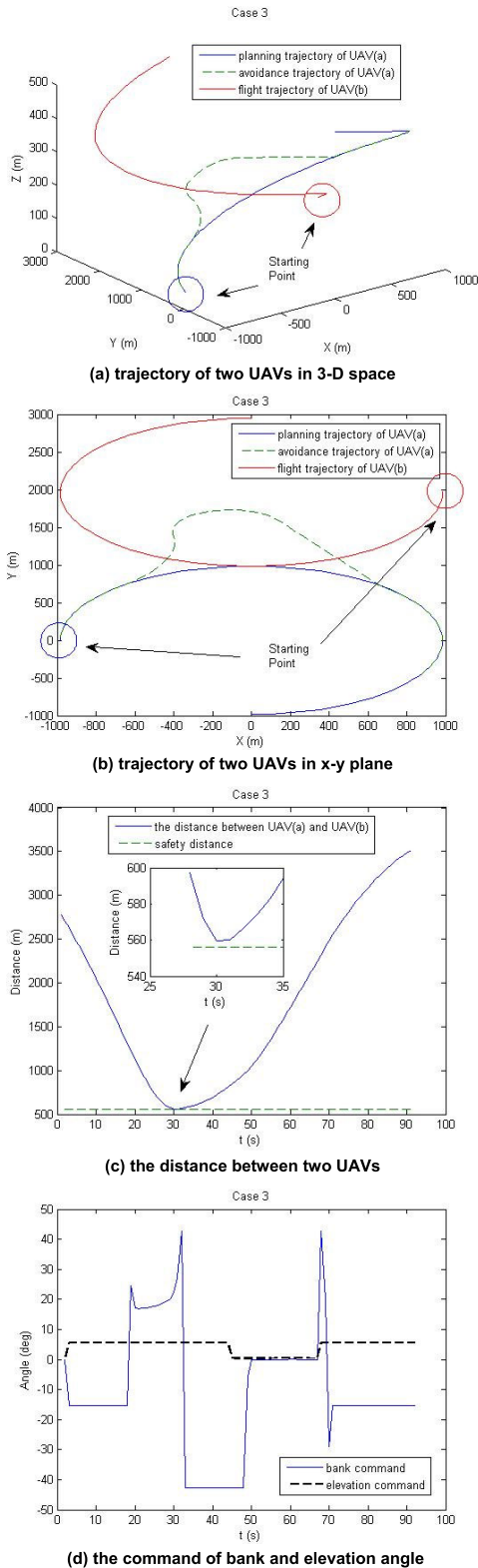


FIGURE 7. Collision avoidance and trajectory recovery in the case 3.

From Fig. 8(a) and 8(b), UAV(b₁) is an obstacle on the flight paths of UAV(a) and UAV(b₂) is an obstacle on the avoidance paths of UAV(a). By using maneuvers only in the horizontal plane, the collision avoidance and trajectory

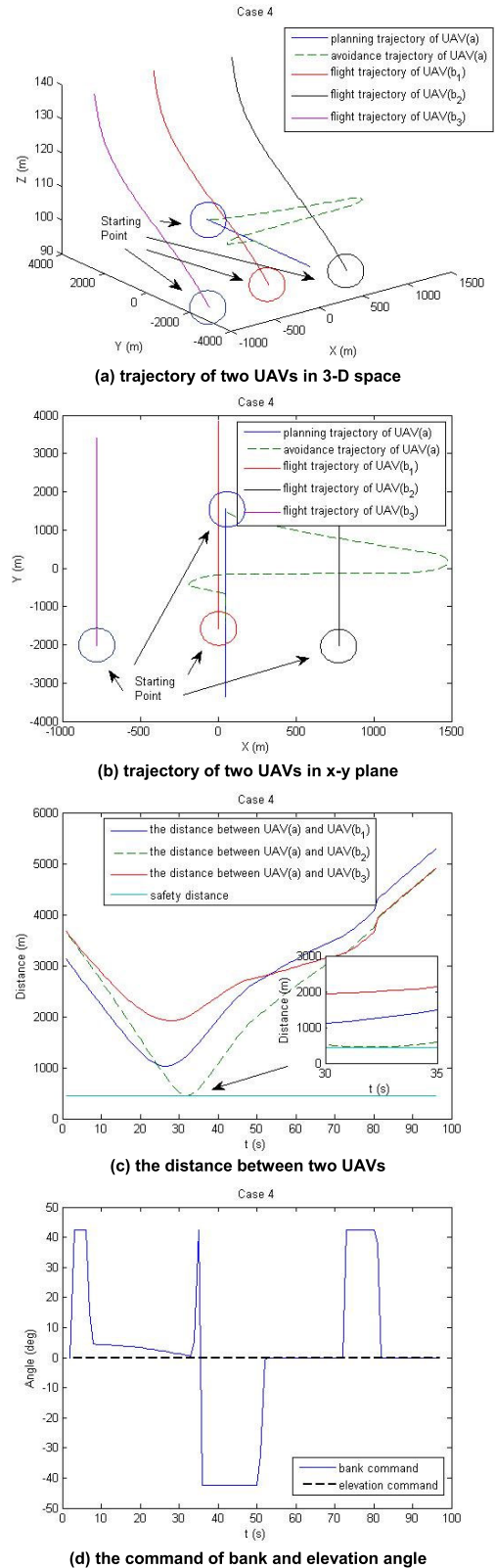


FIGURE 8. Collision avoidance and trajectory recovery in the case 4.

recovery are successfully implemented. From Fig. 8(c), the relative distance is more than the safe radius r_{safe} in whole procedure. The closest distance d_{min} is reached at 32 seconds.

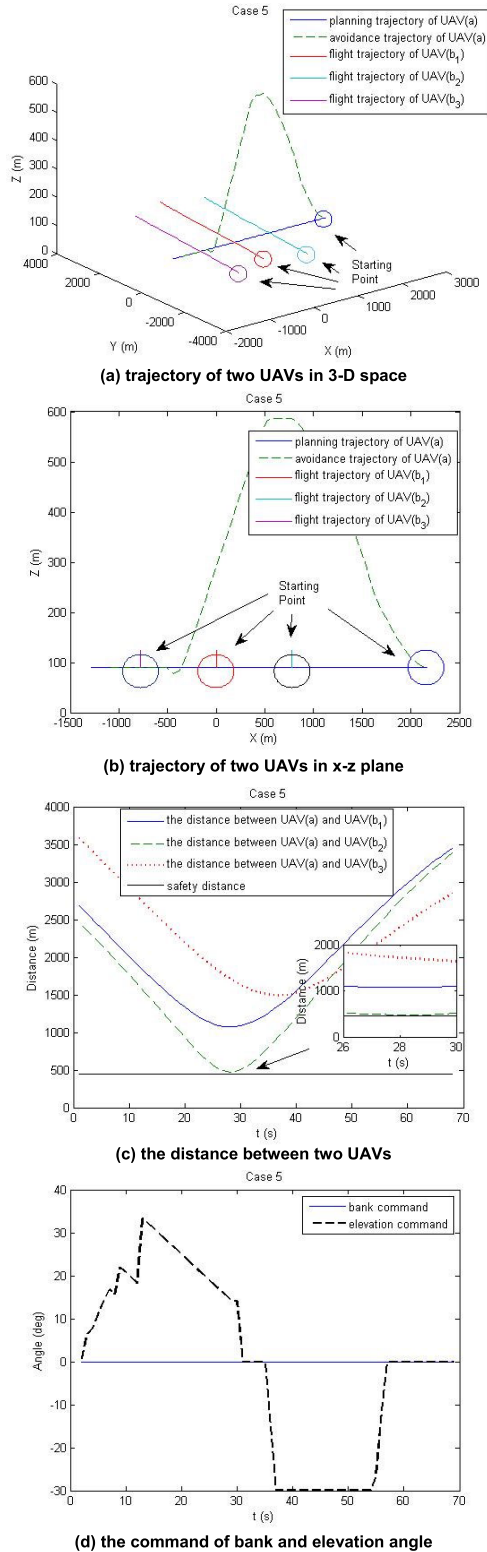


FIGURE 9. Collision avoidance and trajectory recovery in the case 5.

The distance difference ($d_{min} - r_{safe}$) is equal to 4.5 m. From Fig. 8(d), all of commands are in the constraint range. In this scenario, the time expended by the collision avoidance and the trajectory recovery is 32 s and 48 s, respectively.

F. CASE 5

Case 5 is similar with Case 4. However, the initial heading angles of UAV(a) and three intruders is cross in direction. Fig. 9(a) and 9(b) show the flight paths of collision avoidance and trajectory recovery in 3-D and 2-D plane. Fig. 9(c) shows the relative distance between UAV(a) and three intruders. Fig. 9(d) gives the command of bank and elevation angle in whole procedure. From Fig. 9(a) and 9(b), UAV(b₁), UAV(b₂) and UAV(b₃) are three obstacles on the flight paths of UAV(a). By using maneuvers only in the vertical plane, the collision avoidance and trajectory recovery are successfully implemented. From Fig. 9(c), the relative distance is more than the safe radius r_{safe} in whole procedure. The closest distance d_{min} is reached at 28 seconds. The distance difference ($d_{min} - r_{safe}$) is equal to 24.9 m. From Fig. 8(d), all of commands are in the constraint range. In this scenario, the time expended by the collision avoidance and the trajectory recovery is 28 s and 28 s, respectively.

G. CASE 6

In Case 6, UAV(a) is maneuvering in turning paths of the horizontal plane and three intruders (UAV(b₁), UAV(b₂), UAV(b₃)) in formation flight are flight along straight paths. The initial heading angles of UAV(a) and three intruders is parallel in direction. In the horizontal plane, UAV(a) turns right in a constant turning rate. The speed of three intruders is varied and the unknown acceleration is equal to $2 \cos(\pi t/60)$. Fig. 10(a)-10(c) show the flight paths of collision avoidance and trajectory recovery in 3-D and 2-D plane. Fig. 10(d) shows the relative distance between UAV(a) and three intruders. Fig. 10(e) gives the command of bank and elevation angle in whole procedure.

From Fig. 10(a) - 10(c), UAV(b₁), UAV(b₂) and UAV(b₃) are three obstacles on the flight paths of UAV(a). By using maneuvers in both the horizontal and vertical planes, the collision avoidance and trajectory recovery are successfully implemented. From Fig. 10(d), the relative distance is more than the safe radius r_{safe} in whole procedure. The closest distance d_{min} is reached at 256 seconds. The distance difference ($d_{min} - r_{safe}$) is equal to 1.3 m. From Fig. 10(e), all of commands are in the constraint range. In this scenario, the time expended by the collision avoidance and the trajectory recovery is 257 s and 237 s, respectively.

H. CASE 7

In Case 7, the performance of collision avoidance is compared for three methods, i.e. FFTC [32], DAPF [33] and ES proposed in this paper. For Case 7, UAV(a) is flight in spiral paths and UAV(b) is flight in straight paths in the horizontal plane. The initial heading angles of UAV(a) and UAV(b) is opposite in direction. UAV(a) turns right at a constant turning rate. The speed of UAV(b) is varied and the unknown acceleration is equal to $2 \cos(\pi t/60)$. The collision of UAV(a) and UAV(b) will occur in 30 seconds. Fig. 11(a) shows the flight paths of collision avoidance and trajectory

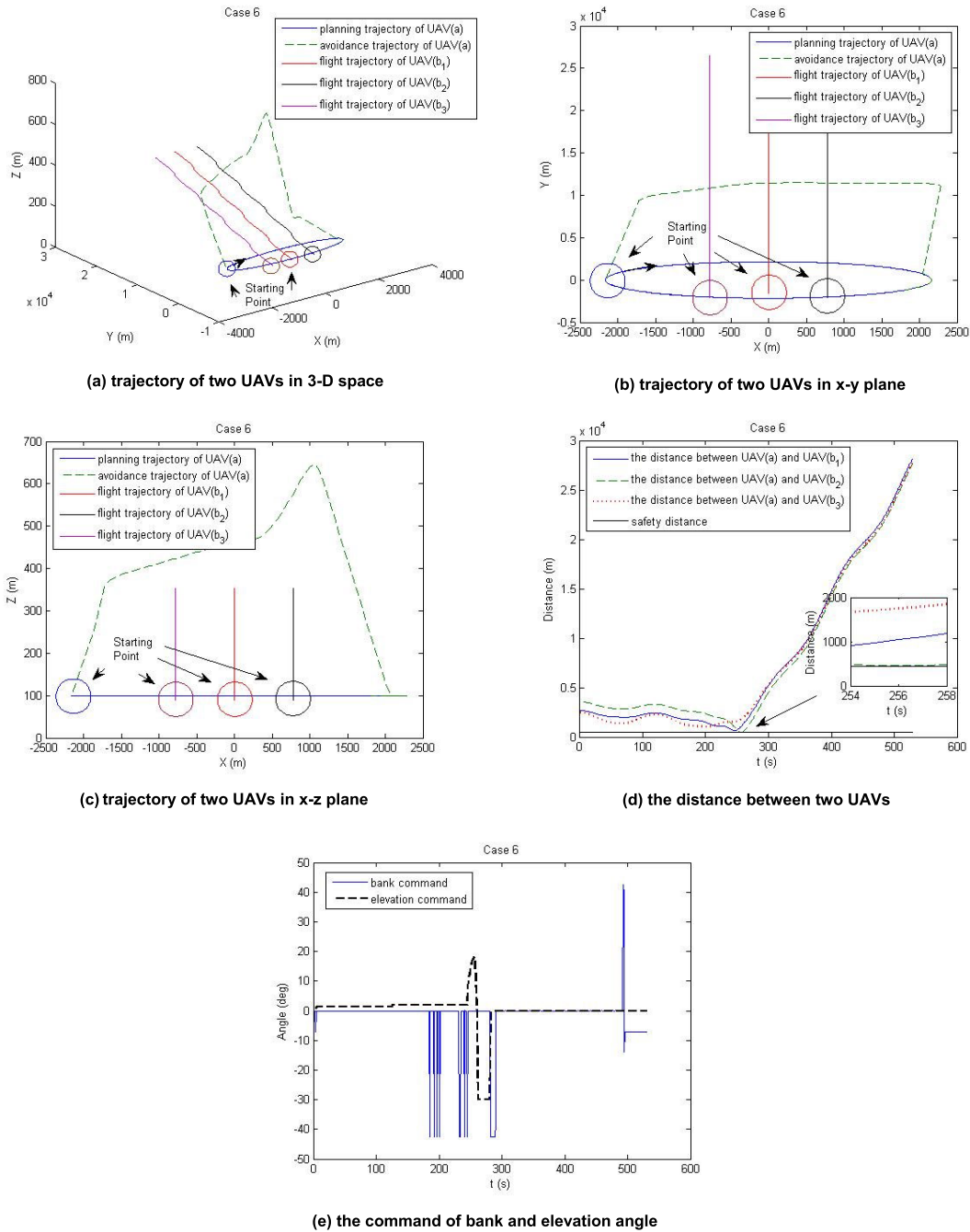


FIGURE 10. Collision avoidance and trajectory recovery in the case 6.

recovery in x-y plane. Fig. 11(b) shows the relative distance between UAV(a) and UAV(b). Fig. 11(c) gives the magnitude of velocity. Fig. 11(d) gives the turning rate of UAV(a). For FFTC, the parameters of algorithm are given by Table 3 in [32]. For DAPF, the parameters of algorithm are $k_p^{att} = 0.1$, $k_v^{att} = 0.1$, $k_p^{rep} = 1700$; $k_v^{rep} = 300$; $k_{damp} = 0.35$; $k_v = 800$; $k_a = 10$; $w_{max} = 10^\circ/s$.

From Fig. 11, three methods can successfully avoid the collision in whole procedure. For FFTC, DAPF and ES, the distance difference ($d_{min} - r_{safe}$) between the closest

distance and the safe radius is equal to 0.5m, 46.9 m and 46.2 m, respectively; and the time expended by the collision avoidance is 24 s, 36 s and 19 s, respectively. After the collision avoidance ends, UAV(a) returns to the planning paths by using ES method. However, UAV(a) does not return to the planning paths when FFTC or DAPF method is used. In three methods, the avoidance trajectory for FFTC is the closest to planning paths. The velocity's magnitude and the turning rate of UAV(a) has the largest fluctuation for DAPF. Its maximum turning rate is more than the limit value of

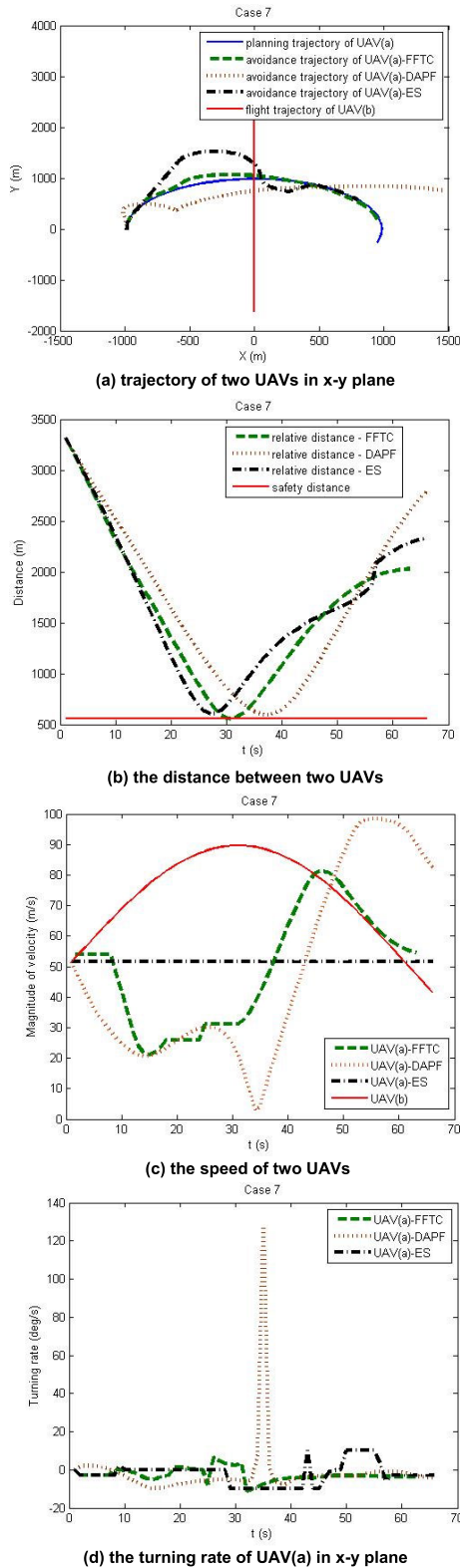


FIGURE 11. Comparison of three methods in the case 7.

turning rate. For ES, the magnitude of velocity is constant and the turning rate is not more than the limit value of turning rate in whole procedure. Comparing with FFTC and DAPF,

TABLE 9. The closest distance of two UAVs for DAPF (unit: m).

UAV(b)\UAV(a)	95(m/s)	97.5	100	102.5	105
95(m/s)	622.6	566.7	493.4	374.2	390.1
97.5	656.2	608.8	548.4	470.8	322.1
100	687.4	644.8	602.9	530.7	446.2
102.5	717.1	675.8	631.9	578.6	513.6
105	741.2	705.6	666.2	618.9	565.5

TABLE 10. The closest distance of two UAVs for FFTC (unit: m).

UAV(b)\UAV(a)	95(m/s)	97.5	100	102.5	105
95(m/s)	555.4	550.9	556.9	552.7	556.7
97.5	555.0	556.2	555.3	553.2	557.1
100	556.6	557.9	556.5	556.7	557.0
102.5	554.7	558.2	547.4	557.8	552.9
105	558.1	553.1	556.4	556.5	556.3

TABLE 11. The closest distance of two UAVs for ES (unit: m).

UAV(b)\UAV(a)	95(m/s)	97.5	100	102.5	105
95(m/s)	606.2	603.3	602.4	610.7	606.8
97.5	604.2	603.3	604.3	607.7	605.1
100	604.1	605.1	602.2	605.9	605.1
102.5	605.8	603.3	600.2	599.1	606.7
105	598.4	601.2	599.9	600.5	610.1

TABLE 12. The comparison of CPU time (unit: $\cdot 10^{-5}$ s).

	FFTC	DAPF	ES
1	380	8.9212	3.0678
2	380	9.0623	3.1030
3	390	8.9565	2.9972
4	390	9.0623	3.2793
5	390	9.2738	2.9620
6	390	8.9212	3.0325
7	390	8.6039	2.9620
8	400	8.8860	2.9972
9	390	9.0270	2.9620
10	390	9.1328	2.9970
Mean value	389	8.9847	3.0360

thus, ES is energy-saving due to no change of velocity's magnitude.

When the initial velocity of UAV(a) or/and UAV(b) has small disturbance, the performance of collision avoidance is compared for three methods. For DAPF, FFTC and ES, the closest distance between UAV(a) and UAV(b) are respectively given in Table 9, 10 and 11, where the initial velocity of UAV(a) varies from 95 m/s to 105 m/s, as shown in the row 1. Similarly, different initial velocity of UAV(b) are shown in the column 1. In Table, the item marking in red boldface type denotes that the closest distance is less than the safe radius (i.e. $r_{safe} = 556$ m). From Table 9, DAPF method cannot avoid the collision successfully in the case that the initial velocity of UAV(a) is more than that of UAV(b) and the initial velocity of UAV(a) is equal to or more than 100 m/s. From Table 10, the collision avoidance fails in 10 cases. This illustrates that the success rate of collision avoidance

is reduced for FFTC method when the initial velocity of UAV(a) or/and UAV(b) has small disturbance. From Table 11, ES method can avoid the collision successfully in all cases. This implies that ES method can ensure the safe flight of UAVs when the initial velocity of UAV(a) or/and UAV(b) has small disturbance. But, FFTC and DAFP methods cannot ensure the safe flight of UAVs in the presence of disturbances.

The comparison of CPU time needed for a Monte Carlo run is shown in Table 12. In all simulations, it is used that MATLAB R2014a on an Intel® Xeon® E3-1225 v6 processor with 3.30 GHz CPU speed. In Table 12, CPU time of running 10 Monte Carlo simulations for the collision avoidance algorithm is recorded and their serial number is 1 to 10. The mean value of CPU time for 10 times is given in final row. From Table 12, CPU time required by ES method is less than that ADPF and FFTC methods. This implies that ES method has lower computational complexity than ADPF and FFTC methods.

IX. CONCLUSION

An effective strategy using mixed 3-D geometric and the miss distance approaches is proposed for the collision avoidance between multiple UAVs with unknown acceleration. For the proposed strategy, the condition required for successful collision avoidance is derived and a simple and feasible modify measure is given to enhance safety during execution of avoidance maneuver. In the case of multiple UAVs, a logic to allocate the avoidance prioritization of each UAV and an algorithm to compute the expected heading and elevation angles of UAV are presented for collision avoidance. The trajectory recovery strategy is proposed to ensure UAV to return to the planning flight paths. The proposed strategy does not constrain that all UAVs have constant ground speeds and direction of the velocity. Thus, it is very suitable in reality application. Numerical simulation results show the proposed strategy can successfully perform the collision avoidance and trajectory recovery for a pair of fixed-wing UAVs or multiple fixed-wing UAVs. Even in the presence of small disturbance, this strategy is also efficacious.

The future work will first explore how to avoid unknown moving obstacles by using the proposed strategy. For this work, it is key issue how to predict the position and velocity information of unknown moving obstacles as accurately as possible. Second, the control algorithm for the horizontal and vertical motions of UAV will be improved to guarantee safe operation in the presence of strong winds. For this work, two approaches should be trialed. One approach is that the wind speed is first estimated. Then, the wind influences on the position and velocity of UAV are compensated by using the estimate of wind speed [36]. Another approach is that the robust controller, such as L_1 adaptive controller [37], should be substituted for traditional PID controller to improve the robust performance against disturbances.

REFERENCES

- [1] J. N. Yasin, S. A. S. Mohamed, M.-H. Haghbayan, J. Heikkinen, H. Tenhunen, and J. Plosila, "Unmanned aerial vehicles (UAVs): Collision avoidance systems and approaches," *IEEE Access*, vol. 8, pp. 105139–105155, 2020.
- [2] J. Tang, S. Lao, and Y. Wan, "Systematic review of collision-avoidance approaches for unmanned aerial vehicles," *IEEE Syst. J.*, vol. 16, no. 3, pp. 4356–4367, Sep. 2022.
- [3] A. Chakravarthy and D. Ghose, "Obstacle avoidance in a dynamic environment: A collision cone approach," *IEEE Trans. Syst., Man, Cybern. A, Syst., Humans*, vol. 28, no. 5, pp. 562–574, Sep. 1998.
- [4] A. Chakravarthy and D. Ghose, "Generalization of the collision cone approach for motion safety in 3-D environments," *Auton. Robots*, vol. 32, no. 3, pp. 243–266, Apr. 2012.
- [5] Y. Xiuxia, Z. Yi, and Z. Weiwei, "Obstacle avoidance method of three-dimensional obstacle spherical cap," *J. Syst. Eng. Electron.*, vol. 29, no. 5, pp. 1058–1068, Oct. 2018.
- [6] C. Y. Tan, S. Huang, K. K. Tan, and R. S. H. Teo, "Three dimensional collision avoidance for multi unmanned aerial vehicles using velocity obstacle," *J. Intell. Robot. Syst.*, vol. 97, no. 1, pp. 227–248, Jan. 2020.
- [7] I. Mahjri, A. Dhraief, A. Belghith, and A. S. AIMogren, "SLIDE: A straight line conflict detection and alerting algorithm for multiple unmanned aerial vehicles," *IEEE Trans. Mobile Comput.*, vol. 17, no. 5, pp. 1190–1203, May 2018.
- [8] J. Krozel and M. Peters, "Conflict detection and resolution for free flight," *Air Traffic Control Quart.*, vol. 5, no. 3, pp. 181–212, Jul. 1997.
- [9] J.-W. Park, H.-D. Oh, and M.-J. Tahk, "UAV collision avoidance based on geometric approach," in *Proc. SICE Annu. Conf.*, Aug. 2008, pp. 2122–2126, doi: 10.1109/SICE.2008.4655013.
- [10] V. Shalunov, "Reciprocal guidance approach for suspicious collision point identification in a multi-agent unmanned aerial vehicle scenario," *Aerosp. Sci. Technol.*, vol. 112, May 2021, Art. no. 106656.
- [11] L.-P. Tsao, C.-L. Chou, C.-M. Chen, and C.-T. Chen, "Aiming point guidance law for air-to-air missiles," *Int. J. Syst. Sci.*, vol. 29, no. 2, pp. 95–102, Feb. 1998.
- [12] J. Park, N. Cho, and S. Lee, "Reactive collision avoidance algorithm for UAV using bounding tube against multiple moving obstacles," *IEEE Access*, vol. 8, pp. 218131–218144, 2020.
- [13] J. Goss, R. Rajvanshi, and K. Subbarao, "Aircraft conflict detection and resolution using mixed geometric and collision cone approaches," in *Proc. AIAA Guid., Navigat., Control Conf. Exhib.*, Aug. 2004, p. 4879. [Online]. Available: <http://arc.aiaa.org/doi/abs/10.2514/6.2004.4879>
- [14] Z. Lin, L. Castano, E. Mortimer, and H. Xu, "Fast 3D collision avoidance algorithm for fixed wing UAVs," *J. Intell. Robot. Syst.*, vol. 97, pp. 577–604, Jun. 2020.
- [15] J. Zhang, J. Yan, and P. Zhang, "Fixed-wing UAV formation control design with collision avoidance based on an improved artificial potential field," *IEEE Access*, vol. 6, pp. 78342–78351, 2018.
- [16] Z.-H. Pang, C.-B. Zheng, J. Sun, Q.-L. Han, and G.-P. Liu, "Distance- and velocity-based collision avoidance for time-varying formation control of second-order multi-agent systems," *IEEE Trans. Circuits Syst. II, Exp. Briefs*, vol. 68, no. 4, pp. 1253–1257, Apr. 2021.
- [17] J. Sun, J. Tang, and S. Lao, "Collision avoidance for cooperative UAVs with optimized artificial potential field algorithm," *IEEE Access*, vol. 5, pp. 18382–18390, 2017.
- [18] Z. Pan, C. Zhang, Y. Xia, H. Xiong, and X. Shao, "An improved artificial potential field method for path planning and formation control of the multi-UAV systems," *IEEE Trans. Circuits Syst. II, Exp. Briefs*, vol. 69, no. 3, pp. 1129–1133, Mar. 2022.
- [19] J. Li, Y. Fang, H. Cheng, Z. Wang, Z. Wu, and M. Zeng, "Large-scale fixed-wing UAV swarm system control with collision avoidance and formation maneuver," *IEEE Syst. J.*, vol. 17, no. 1, pp. 744–755, Mar. 2023.
- [20] P. Pierpaoli and A. Rahmani, "UAV collision avoidance exploitation for noncooperative trajectory modification," *Aerosp. Sci. Technol.*, vol. 73, pp. 173–183, Feb. 2018.
- [21] J. Yang, D. Yin, Q. Cheng, and L. Shen, "Two-layered mechanism of online unmanned aerial vehicles conflict detection and resolution," *IEEE Trans. Intell. Transp. Syst.*, vol. 19, no. 10, pp. 3230–3244, Oct. 2018.
- [22] A. Hendrickson, "An investigation of alerting and prioritization criteria for sense and avoid (SAA)," U.S. Army Res., Redstone Arsenal, AL, USA, Tech. Rep. RDMR-TM-13-01, 2013.

- [23] J. Seo, Y. Kim, S. Kim, and A. Tsourdos, "Collision avoidance strategies for unmanned aerial vehicles in formation flight," *IEEE Trans. Aerosp. Electron. Syst.*, vol. 53, no. 6, pp. 2718–2734, Dec. 2017.
- [24] Y. Huang, J. Tang, and S. Lao, "Collision avoidance method for self-organizing unmanned aerial vehicle flights," *IEEE Access*, vol. 7, pp. 85536–85547, 2019.
- [25] Y. Wan, J. Tang, and S. Lao, "Distributed conflict-detection and resolution algorithm for UAV swarms based on consensus algorithm and strategy coordination," *IEEE Access*, vol. 7, pp. 100552–100566, 2019.
- [26] J. Tang, G. Liu, and Q. Pan, "A review on representative swarm intelligence algorithms for solving optimization problems: Applications and trends," *IEEE/CAA J. Autom. Sinica*, vol. 8, no. 10, pp. 1627–1643, Oct. 2021.
- [27] J. Tang, X. Chen, X. Zhu, and F. Zhu, "Dynamic reallocation model of multiple unmanned aerial vehicle tasks in emergent adjustment scenarios," *IEEE Trans. Aerosp. Electron. Syst.*, vol. 59, no. 2, pp. 1139–1155, Apr. 2023, doi: [10.1109/TAES.2022.3195478](https://doi.org/10.1109/TAES.2022.3195478).
- [28] S. He, C. Dong, S. Dai, and T. Zou, "Cooperative deterministic learning and formation control for underactuated USVs with prescribed performance," *Int. J. Robust Nonlinear Control*, vol. 32, no. 5, pp. 2902–2924, Mar. 2022, doi: [10.1002/rnc.5871](https://doi.org/10.1002/rnc.5871).
- [29] K. Cole and A. M. Wickenheiser, "Reactive trajectory generation for multiple vehicles in unknown environments with wind disturbances," *IEEE Trans. Robot.*, vol. 34, no. 5, pp. 1333–1348, Oct. 2018.
- [30] J. Feng, J. Zhang, G. Zhang, S. Xie, Y. Ding, and Z. Liu, "UAV dynamic path planning based on obstacle position prediction in an unknown environment," *IEEE Access*, vol. 9, pp. 154679–154691, 2021.
- [31] S. X. Wei, A. Dixit, S. Tomar, and J. W. Burdick, "Moving obstacle avoidance: A data-driven risk-aware approach," *IEEE/CSS Control Syst. Lett.*, vol. 7, pp. 289–294, Apr. 2023.
- [32] N. Zhang, W. Gai, M. Zhong, and J. Zhang, "A fast finite-time convergent guidance law with nonlinear disturbance observer for unmanned aerial vehicles collision avoidance," *Aerosp. Sci. Technol.*, vol. 86, pp. 204–214, Mar. 2019.
- [33] Y. Du, X. Zhang, and Z. Nie, "A real-time collision avoidance strategy in dynamic airspace based on dynamic artificial potential field algorithm," *IEEE Access*, vol. 7, pp. 169469–169479, 2019.
- [34] L. Zhu, Y. Wang, and Z. Wu, "An adaptive priority allocation for formation UAVs in complex context," *IEEE Trans. Aerosp. Electron. Syst.*, vol. 57, no. 2, pp. 1002–1015, Apr. 2021.
- [35] D. P. Jack, K. D. Hoffler, and S. C. Johnson, "Evaluation of the trade space between UAS maneuver performance and SAA system performance requirements," NASA Center AeroSpace Inf. Standard Drive Hanover, Hanover, MD, USA, Tech. Rep. NASA/CR-2014-218264, 2014.
- [36] Y. Yang, X. Liu, X. Liu, Y. Guo, and W. Zhang, "Model-free integrated navigation of small fixed-wing UAVs full state estimation in wind disturbance," *IEEE Sensors J.*, vol. 22, no. 3, pp. 2771–2781, Feb. 2022.
- [37] T. Souaneif, " \mathcal{L}_1 adaptive path-following of small fixed-wing unmanned aerial vehicles in wind," *IEEE Trans. Aerosp. Electron. Syst.*, vol. 58, no. 4, pp. 3708–3716, Aug. 2022.



JIANWU TAO received the M.Sc. degree in electronic engineering and the Ph.D. degree in communication engineering from Jilin University, Changchun, China, in 1989 and 2004, respectively. He is currently a Full Professor. His research interests include unmanned aerial vehicle systems and control, and signal processing.



SHIRU GUO received the M.E. degree in material processing engineering from the Changchun University of Science and Technology, China, in 2009. She is currently an Associate Professor. Her research interest includes unmanned aerial vehicle systems and simulation.

YUFENG SHANG received the B.Sc. degree in system engineering from the National University of Defense Technology, China, in 1988, and the M.E. and Ph.D. degrees from Jilin University, China, in 2004 and 2010, respectively. She is currently a Full Professor. Her research interests include unmanned aerial vehicle systems and modeling.

• • •